Pervasive exsolution within the calcic amphibole series: TEM evidence for a miscibility gap between actinolite and hornblende in natural samples

Eugene A. Smelik

Department of Earth and Planetary Sciences, The Johns Hopkins University, Baltimore, Maryland 21218, U.S.A.

Matthew W. Nyman

Department of Geological Sciences, Virginia Polytechnic Institute and State University, Blacksburg, Virginia 24061, U.S.A.

David R. Veblen

Department of Earth and Planetary Sciences, The Johns Hopkins University, Baltimore, Maryland 21218, U.S.A.

Abstract

Transmission and analytical electron microscope (TEM/AEM) study of complex calcic amphibole assemblages in metagabbros from the Cheyenne belt, southeast Wyoming, has revealed the amphiboles to be pervasively exsolved on a very fine scale.

Electron microprobe analyses indicate that the bulk composition of the amphiboles ranges from actinolite ($Al_{tot} = 0.559$) to magnesio-hornblende ($Al_{tot} = 2.587$). AEM analyses of the exsolved phases show them to be actinolite with an average composition of $K_{0.03}Na_{0.12}(Na_{0.18}Ca_{1.71}Fe_{0.08}Mn_{0.03})(Fe_{1.55}Mg_{3.05}Al_{0.38}Ti_{0.02})[Al_{0.38}Si_{7.62}]O_{22}(OH)_2$ and hornblende with an average composition of $K_{0.14}Na_{0.36}(Ca_{1.88}Fe_{0.16}Mn_{0.02})(Fe_{2.4}Mg_{1.8}Al_{0.76}-Ti_{0.05})[Al_{1.48}Si_{6.52}]O_{22}(OH)_2$. The tschermakite exchange, $^{[6]}Al,^{[4]}Al \leftrightarrow (Mg,Fe),Si$, predominates during the exsolution process, accompanied by minor edenite exchange, $Na^A,^{[4]}Al \leftrightarrow \square,Si$. The hornblendes are always significantly richer in Fe and have a higher A-site occupancy than the actinolites.

The exsolution microstructure occurs as a pervasive fine-scale tweed texture with lamellae typically on the order of 5–15 nm thick. The coarsest lamellae occur in compositional zones representing the middle of the actinolite-hornblende solvus, whereas increasingly finer textures are observed on both limbs. High-resolution TEM images indicate that the microstructure is coherent with diffuse lamellar interfaces. The lamellae occur in two symmetrical orientations, nearly parallel to ($13\bar{2}$) and ($1\bar{3}2$). Since the unit-cell dimensions of the exsolved phases are so similar, these orientations are somewhat variable. The orientation of this microstructure differs significantly from more common lamellar orientations ("100" and "$\bar{1}01$") in exsolved monoclinic amphiboles. Optimal phase boundary calculations using EPLAG successfully predict the observed orientation for selected combinations of unstrained actinolite-hornblende lattice parameters. More importantly, they show that optimal phase boundaries may occur over a wide range of orientations depending upon actual differences in the two lattices, which are sensitive functions of composition and perhaps pressure and temperature.

Selected-area electron diffraction (SAED) patterns of coarse tweed areas have revealed small satellite spots around the main Bragg reflections, indicating that the microstructure is relatively periodic, with measured periodicities ranging from 25 to 35 nm. The small satellite spots around single reciprocal lattice points, pervasive tweed texture, diffuse lamellar interfaces, and small size of the exsolution lamellae are consistent with a spinodal decomposition mechanism.

Introduction

The existence and characterization of the miscibility gap within the calcic amphibole series has been the subject of much study and even debate over the last 20 years. Numerous petrographic, petrologic, and mineralogic studies have described a wide range of coexisting actinolite-hornblende assemblages from very diverse geologic settings (e.g., Miyashiro, 1958; Shido and Miyashiro, 1959; Klein, 1969; Cooper and Lovering, 1970; Brady, 1974; Graham, 1974; Hietanen, 1974; Grapes, 1975; Misch and Rice, 1975; Tagiri, 1977; Allen and Goldie, 1978; Grapes and Graham, 1978; Cho et al., 1988; Kimball, 1988). Many workers have postulated a miscibility gap between coexisting actinolite and hornblende on the basis of sharp optical and chemical discontinuities and the systematic partitioning of elements between the minerals (e.g., Miyashiro, 1958; Klein, 1969; Cooper and Lovering, 1970;

Brady, 1974; Tagiri, 1977). Other studies have argued against the gap based on the common observation of irregular, patchy intergrowths and overgrowth textures, as well as continuous compositional gradients with changing metamorphic grade in some coexisting actinolite-hornblende assemblages (e.g., Ernst, 1972; Graham, 1974; Grapes, 1975; Sampson and Fawcett, 1977). Grapes and Graham (1978) addressed the fundamental question of whether the complex range of observed actinolite-hornblende intergrowths truly represents equilibrium crystallization and therefore a miscibility gap. They demonstrated that, at least in some cases, the coexisting amphiboles were most likely the result of disequilibrium processes and kinetically hindered crystallization accompanying changing metamorphic conditions rather than a miscibility gap. They further stressed the important effects of other mineral phases on the amphibole compositions. Clearly, the demonstration of true immiscibility between coexisting actinolite-hornblende remains problematic.

Robinson et al. (1982) state that "the presence of one set of amphibole lamellae in another is one of the surest and soundest pieces of evidence for a crystal-chemically controlled miscibility gap and coexisting amphiboles." Unfortunately, unequivocal evidence of exsolution between actinolite and hornblende has yet to be characterized. Cooper and Lovering (1970) reported exsolution lamellae in calcic amphiboles from the Haast River schists that later turned out to be twin lamellae (Cooper, 1972). Klein (1969) reported "100" and "$\bar{1}01$" exsolution lamellae in hornblendes coexisting with actinolite in rocks from Madagascar; he suggested that the lamellae might be actinolite, although they were not analyzed.

Experimental studies of calcic amphibole solid solutions have yielded contradicting results with regard to the actinolite-hornblende miscibility gap. The studies by Oba (1980) and Oba and Yagi (1987) on the tremolite-pargasite join and the actinolite-pargasite join, respectively, have shown well-defined solvi between tremolite and pargasite at 1 kbar and 800 °C and actinolite and pargasite at 1 kbar and 680 °C, with the gap becoming narrower with increasing Fe content.

Jenkins (1988) studied compositions along the tremolite-tschermakite join at 12 kbar, 850 °C and at 3 kbar, 850 °C. His 12 kbar experiments indicated amphibole solid solutions between Ts_0Tr_{100} and $Ts_{50}Tr_{50}$, and the 3 kbar experiments showed a more restricted range of solid solution between Ts_0Tr_{100} and $Ts_{10}Tr_{90}$. However, none of the experimental results showed evidence of immiscibility between two amphiboles along this join at these P-T conditions. The work of Moody et al. (1983) on the greenschist-amphibolite transition showed fairly smooth compositional changes (increasing Al content) in calcic amphiboles with increasing temperature (400–550 °C) at 2 and 4 kbar. The high-temperature solution calorimetry study of fluor-amphiboles along the fluor-tremolite–fluor-edenite join by Graham and Navrotsky (1986) also provided no evidence of immiscibility within the calcic amphibole series. Graham et al. (1989) have recently re-

viewed some of the important uncertainties associated with experimental studies of amphiboles and the application of experimental results to natural systems.

The purpose of the present paper is to present detailed chemical and crystallographic characterization of exsolution involving actinolite and hornblende observed in complex calcic amphibole assemblages in metagabbros from the Cheyenne belt, southeast Wyoming. We believe that these results constitute a convincing argument for a miscibility gap within the calcic amphibole series.

GEOLOGIC SETTING AND SAMPLE DESCRIPTION

The actinolite-hornblende exsolution texture is observed in amphiboles from a variably deformed amphibolite boudin in the Cheyenne belt, southeast Wyoming. The Cheyenne belt is a crustal-scale shear zone that extends across southeastern Wyoming from the Laramie Range in the east through the Medicine Bow Mountains to the Sierra Madre Range. The belt marks the boundary between the Archean Wyoming Province greenschist-facies basement and younger supracrustals (2300–2000 Ma) to the north and middle- to upper-amphibolite facies Proterozoic terranes of the Colorado Province (1800 Ma) of the Front Range in the south (Duebendorfer and Houston, 1987). The Cheyenne belt is characterized by intense deformation, localized in shear zones along the margins of a series of lithotectonic blocks, which accompanied Proterozoic accretionary tectonics. Metamorphic conditions estimated from synkinematic porphyroblasts indicate that thrusting occurred at a minimum temperature of 475 °C at a pressure of 3 kbar (Duebendorfer, 1988). Temperature estimates of approximately 500 °C were calculated for our specimens using amphibole-plagioclase exchange in variably deformed amphibolite (Nyman et al., 1989). Synkinematic granites and cross-cutting plutons indicate that Cheyenne belt deformation occurred at about 1750 Ma (Duebendorfer and Houston, 1987).

The amphibolite boudin is located within the East Bear Lake Block in the Medicine Bow Mountains (see Fig. 3 of Duebendorfer and Houston, 1987) and shows a well-developed strain transition from undeformed or weakly lineated amphibolite to intensely foliated and lineated, fine-grained amphibolite. The actinolite-hornblende exsolution texture has been studied only in the least deformed amphibolite. This amphibolite has a subophitic texture with plagioclase interstitial to amphibole. Other minerals in the amphibolite include ilmenite, titanite, epidote, and quartz. In thin section, the plagioclase feldspar shows abundant evidence of crystal-plastic deformation, including grain size reduction, undulatory extinction, and the development of core-mantle structures. Amphibole occurs in large, 4- to 6-mm clots that consist of a large, pale green, inclusion-rich core (which may represent a relict phenocryst), rimmed by blue-green, equant amphiboles and thin, undeformed amphibole needles (Fig. 1). Amphibole porphyroclasts show evidence of mechanical twinning and undulatory extinction. The blue-green equant

Fig. 1. Plane polarized light micrograph of complex amphibole assemblage in the least deformed amphibolite boudin. The amphiboles occur as large, inclusion-filled porphyroclasts (1), equant subgrains (2), and postkinematic needles (3). The inset shows a higher magnification backscattered electron image of the subgrains (boxed area) containing narrow "100" and "$\bar{1}01$" cummingtonite lamellae (arrows). The porphyroclasts and subgrains were found to contain pervasive actinolite-hornblende exsolution.

amphiboles have been interpreted as subgrains that formed during deformation and recrystallization of the amphibolite boudin, whereas the amphibole needles are postkinematic. Compositional profiles across the amphibole porphyroclasts, subgrains, and needles show an increase in tschermakitic and edenitic exchange components, which indicates that the texture formed during prograde conditions (Nyman et al., 1989).

EXPERIMENTAL TECHNIQUES

The complex calcic amphibole assemblages were studied using transmission and analytical electron microscopy (TEM/AEM) and electron microprobe analysis (EMP). TEM samples were prepared by ion thinning selected areas of petrographic thin sections. Both the porphyroclasts and equant subgrains were examined in the TEM. Electron microscopy was performed at Johns Hopkins University with a Philips EM420 transmission electron microscope operated at 120 keV. A SuperTwin (ST) objective lens (spherical aberration coefficient $C_s = 1.2$ mm, chromatic aberration coefficient $C_c = 1.2$ mm) was used. For high-resolution (HRTEM) imaging, the objective aperture diameter either matched the point resolution of the mi-

croscope (0.30 nm) or was smaller in order to eliminate irrelevant high-frequency information from the images.

Energy-dispersive X-ray spectra (EDS) were obtained with an EDAX SiLi detector and processed with a Princeton Gamma-Tech model 4000 analyzer, as described by Livi and Veblen (1987, Appendix 2).

Quantitative chemical analysis of amphibole was carried out on a Cameca SX-50 fully automated, four spectrometer electron microprobe at Virginia Polytechnic Institute and State University. Operating conditions were 15 kV and 20 nA. The following mineral standards were used for the microprobe analyses: Na_2O, SiO_2, Al_2O_3: Amelia albite; K_2O: Benson orthoclase; MgO: norbergite; MnO: pyrolusite; TiO_2: rutile; CaO: wollastonite; FeO: Rockport fayalite. Compositional data were corrected using a ZAF program supplied by Cameca.

TEM RESULTS

Morphology, distribution, and diffraction effects from the exsolution lamellae

The only evidence of exsolution from optical and EMP examination of these samples was the common observation of narrow lamellae nearly parallel to (100) and

TABLE 1. Representative AEM analyses for cummingtonite lamellae

Sample no. Spectrum no.		62F 2B6B	62F 2F37B	62F 2F21B	62F 2F44B	62F 2F46B	62F 2F63B
Tetrahedral sites	Si	7.865	7.896	7.839	7.861	7.985	7.834
	Al	0.135	0.104	0.161	0.139	0.015	0.166
	Σ T site	8.000	8.000	8.000	8.000	8.000	8.000
M(1, 2, 3)	Al	0.043	0.025	0.034	0.013	0.058	0.021
	Ti	0.000	0.003	0.000	0.015	0.019	0.000
	Mg	3.498	3.387	3.245	3.521	3.598	3.436
	Fe^{2+}	1.459	1.584	1.721	1.451	1.324	1.543
	Σ M(1, 2, 3)	5.000	4.999	5.000	5.000	4.999	5.000
M(4)	Ca	0.081	0.092	0.090	0.143	0.115	0.080
	Na	0.142	0.023	0.043	0.071	0.119	0.084
	Fe^{2+}	1.615	1.691	1.655	1.619	1.619	1.659
	Mn	0.162	0.194	0.212	0.167	0.147	0.178
	Σ M(4)	2.000	2.000	2.000	2.000	2.000	2.001
A site	Na	0.221	0.095	0.156	0.165	0.034	0.216
	K	0.013	0.000	0.015	0.002	0.002	0.013
	Σ A site	0.234	0.095	0.171	0.167	0.036	0.229
$Fe^{2+}/(Fe^{2+} + Mg)$		0.468	0.492	0.510	0.466	0.450	0.482

Note: Amphibole formula based on normalization to 23 O atoms and assuming all FeO.

($\bar{1}01$) in the amphibole subgrains (Fig. 1). These lamellae appear identical to the commonly reported occurrences of cummingtonite exsolution lamellae in calcic amphiboles (e.g., Vernon, 1962; Robinson, 1963; Jaffe et al., 1968; Ross et al., 1968; Robinson et al., 1969; Ross et al., 1969). AEM analyses (Table 1) and selected-area electron diffraction (SAED) patterns of these lamellae indicate that they are indeed $C2/m$ cummingtonite.

When examined in the TEM, an exsolution microstructure of much finer scale was found to exist in these amphiboles. The microstructure occurs as a pervasive tweed structure (Fig. 2) and is typical of fine-scale exsolution microstructures found in many silicates (see below). The exsolution lamellae occur in two orientations and are very narrow, ranging from 5 to 15 nm in thickness in the relatively coarse tweed areas. Conventional amplitude-contrast (CTEM) and high-resolution (HRTEM) electron microscope images indicate that the interfaces between lamellae in the dense tweed areas are coherent and somewhat diffuse and curved (Figs. 2 and 3). The degree of coarseness of the tweed microstructure varies from grain to grain and in some cases within single grains, reflecting different bulk compositions and chemical zoning. In addition to differences in chemistry leading to variations in coarseness of the microstructure, coarsening of the tweed structure is also observed at dislocations, grain boundaries, and at the interfaces of the "100" and "$\bar{1}01$" cummingtonite lamellae (Figs. 4 and 5). These observations suggest that the formation of the tweed structure postdates the cummingtonite exsolution and at least some of the deformation.

SAED patterns of the coarse tweed areas indicate that a single reciprocal lattice with small satellite spots surrounds the main Bragg reflections (Fig. 6). This observation is consistent with spinodal decomposition (Champness and Lorimer, 1976), although it is not absolute proof that this was the exsolution mechanism. The lack of distinct splitting of the strong Bragg reflections

attests to the similarity of unit-cell parameters for the two amphiboles. The presence of the satellite reflections indicates that the microstructure is reasonably periodic, with measured periodicities ranging from 25 to 35 nm. The tweed microstructure in these amphiboles is very similar to tweed exsolution structures observed in pyroxenes (e.g., Christie et al., 1971; Champness and Lorimer, 1971, 1976; Nord et al., 1976), plagioclase feldspars (e.g., McConnell, 1974; Nord et al., 1974), and alkali feldspars (e.g., McConnell, 1969; Owen and McConnell, 1974), which are thought to have formed by spinodal decomposition. In very fine tweed areas (Fig. 2d), these distinct satellite spots degrade into streaks of diffuse intensity, suggesting a more poorly developed periodicity. This may reflect compositional modulations of lower amplitude accompanying the onset of spinodal decomposition, as opposed to higher amplitude modulations in the coarsened areas.

Orientation of the exsolution lamellae

For the following discussion, all crystallographic directions and planar orientations will be given in terms of the $C2/m$ unit-cell setting for monoclinic amphiboles. The relationships between the $C2/m$ unit-cell setting and the $I2/m$ unit-cell setting are discussed by Whittaker and Zussman (1961), Jaffe et al. (1968), and Thompson (1978).

The simplest way to determine the orientation of submicroscopic exsolution lamellae is to obtain a sample geometry that allows the lamellae to be viewed at an angle perpendicular to their short dimension, that is, edge on. The diffuse nature of lamellar interfaces in this microstructure makes recognition of the edge-on orientation rather difficult even in the coarse tweed areas. It is obvious from Figure 2, however, that the lamellae appear to be much closer to the proper orientation when viewed down [101] (Fig. 2a) as opposed to [010] (Fig. 2b). One area of anomalously coarse lamellae approaching 30–40 nm in thickness was found, which allowed a relatively accurate determination of the orientation (Fig. 7). Figure 7a illus-
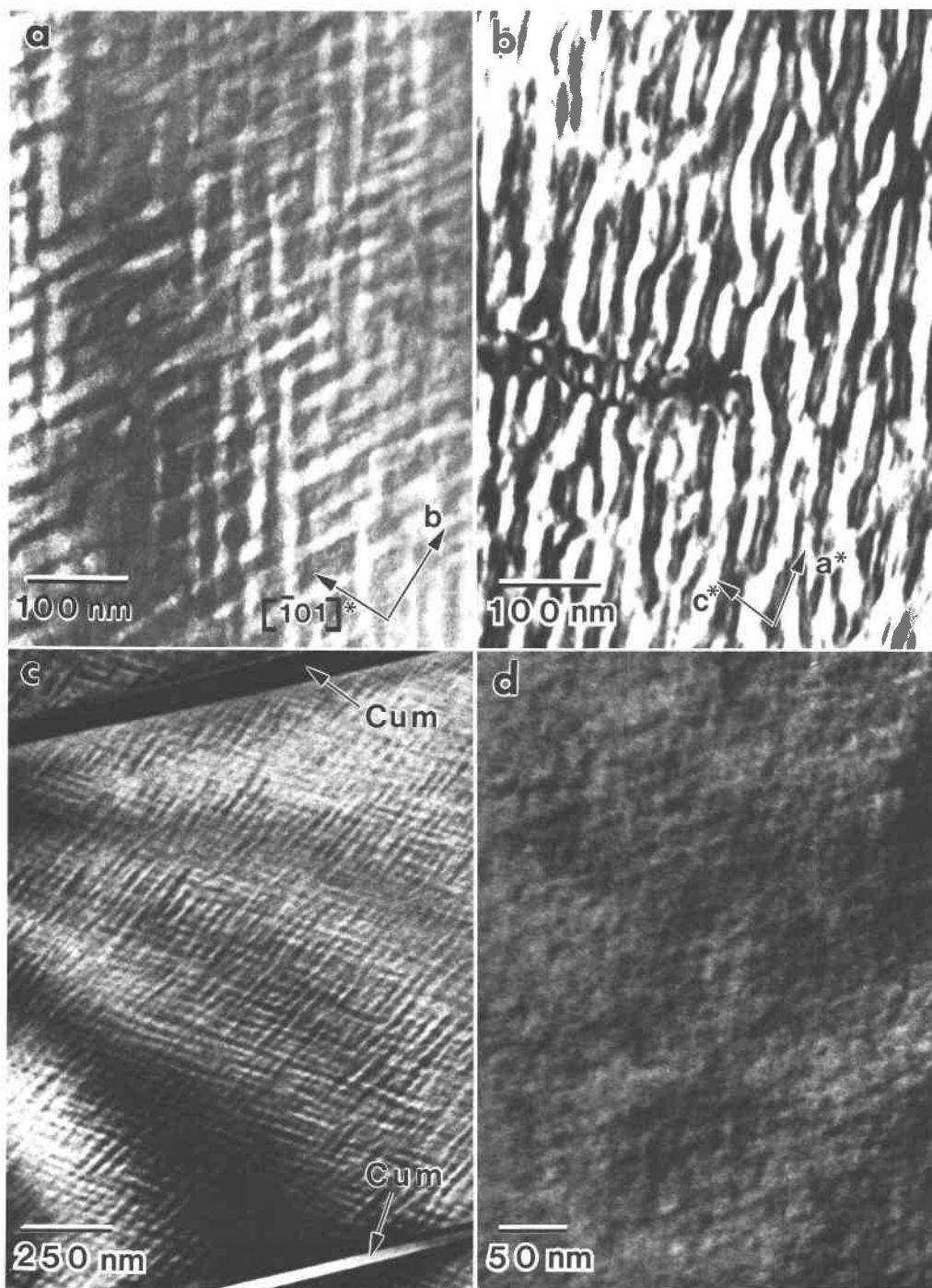
Fig. 2. Bright field TEM images of pervasive tweed exsolution textures in complex calcic amphiboles (**a**) Coarse tweed texture in a large porphyroclast viewed down [101]. Note that the compositional modulations occur in two symmetrical orientations. (**b**) Coarse tweed in a subgrain viewed parallel to **b.** The lamellar interfaces appear curved in this highly tilted orientation. (**c**) Pervasive tweed exsolution with two larger, "100" cummingtonite lamellae. This area is tilted out of a zone-axis orientation. (**d**) Fine-scale tweed texture in an actinolitic subgrain, which probably represents the initial stages of spinodal decomposition. Electron beam is parallel to [101].
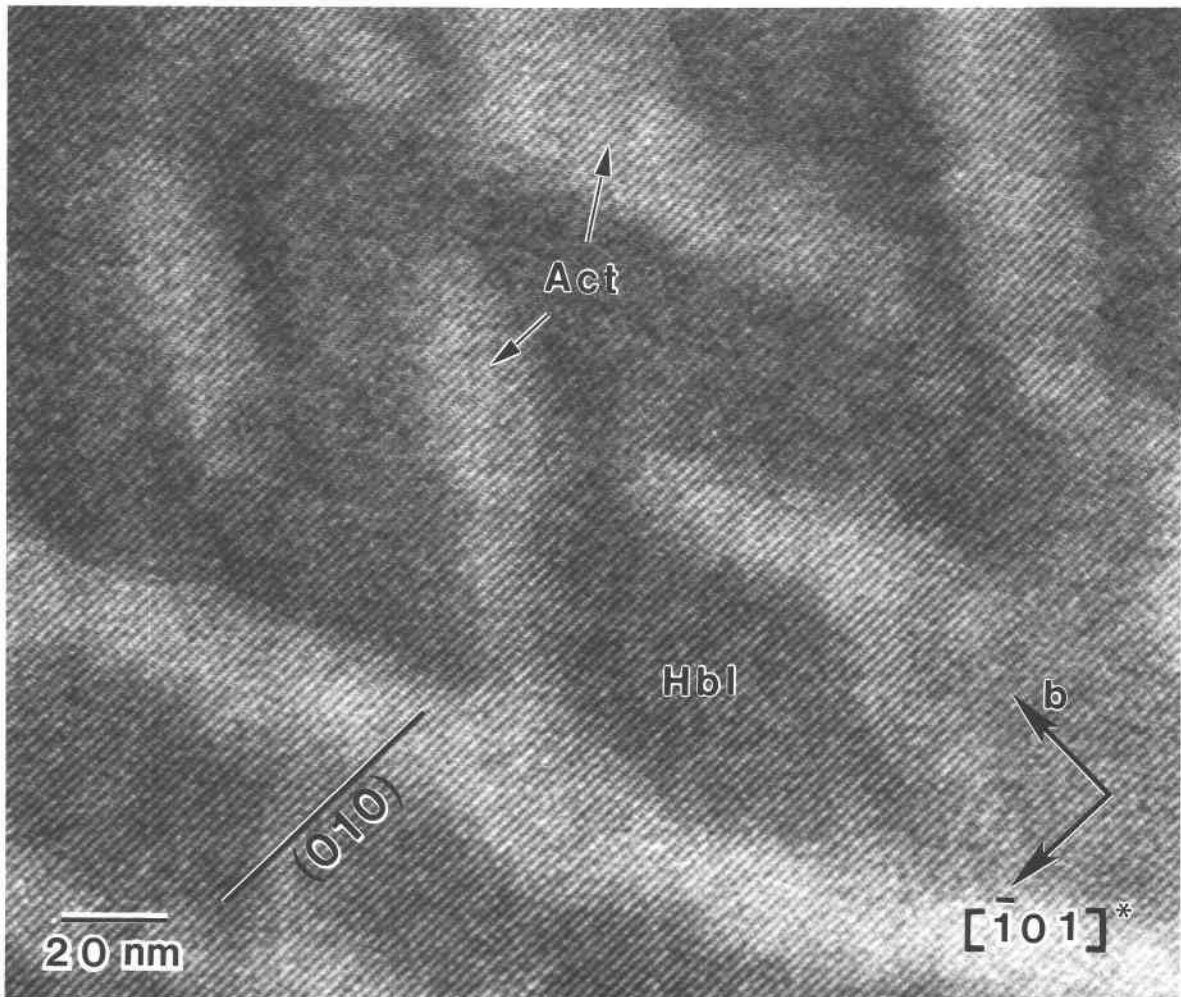
Fig. 3. HRTEM image of coarse tweed area taken down the [101] zone. The microstructure is coherent, with no disruption of the (020) lattice fringes. Note the diffuse nature of the lamellar interfaces.

trates a view down the [201] zone of this coarse area. Note that the two sets of lamellae have relatively sharp, straight interfaces, suggesting that they are oriented with their shortest dimensions nearly parallel to the plane of the photograph. Figure 7b shows the SAED pattern for the [201] zone, which contains $\mathbf{b}^*$ and $[\bar{1}12]^*$. It is evident that the two sets of lamellae are symmetrically related by the mirror plane normal to $\mathbf{b}$. Since any reciprocal lattice vector, $\mathbf{r}^*_{hkl}$, is perpendicular to the planes, (hkl), with the same indices, the lamellar orientations may be found by identifying the appropriate $\mathbf{r}^*_{hkl}$'s in the SAED pattern. This procedure is illustrated in Figure 7. Note that the vectors $[13\bar{2}]^*$ and $[1\bar{3}2]^*$ are nearly perpendicular to the two sets of lamellae, so the lamellae may be designated "13$\bar{2}$" and "1$\bar{3}2$." The true orientations of the lamellae are really parallel to planes with irrational indices, and because the unit cells of the actinolite and hornblende are so similar in dimensions, this orientation may be quite variable, depending upon small compositional differences.

These unusual orientations are significantly different

from the typical "100" and "$\bar{1}01$" lamellae commonly observed in mutually exsolved calcic and ferromagnesian amphiboles (see Figs. 2c and 5 and references above). Work by Robinson et al. (1971, 1977) has shown that the "100" and "$\bar{1}01$" phase boundaries are actually irrational and can be called "optimal phase boundaries" (terminology of Bollman and Nissen, 1968). It has been well established that the magnitude of the dimensional (or structural) misfit between two coherently intergrown crystal lattices is the dominant factor controlling the exact orientations of optimal phase boundaries (Cahn, 1968; Bollman and Nissen, 1968; Robinson et al., 1971, 1977; Willaime and Brown, 1974; Robin, 1974, 1977; Fleet et al., 1980; Fleet, 1982). Robinson and coworkers further showed that lamellar orientations in clinoamphiboles and pyroxenes are usually constrained by the "exact phase boundary theory," providing the b axial lengths of the two structures are nearly identical (Robinson et al., 1971, 1977). Since the present lamellar orientations differ from "100" and "$\bar{1}01$," it seems likely that they are not constrained
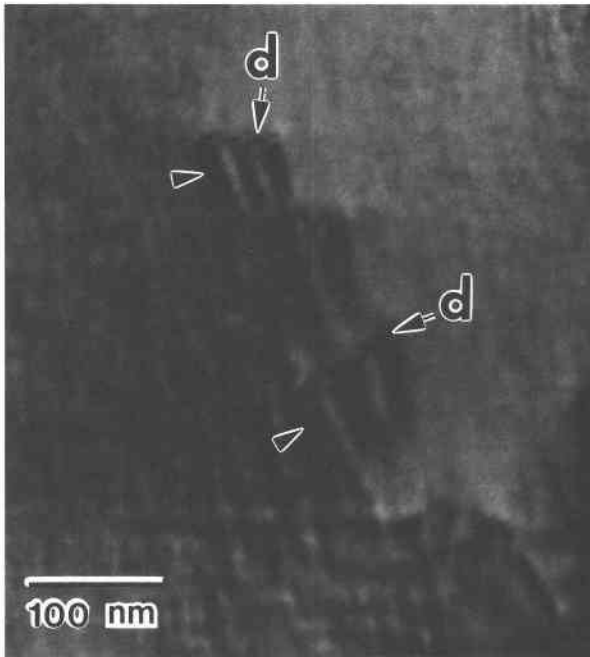
Fig. 4. Bright field TEM image of fine-scale tweed exsolution with coarsening (arrows) at dislocations (d). These dislocations may be heterogeneous nucleation sites. A nonzone-axis orientation was used to enhance contrast.

by this theory and that the magnitudes of the b axes of the actinolite and hornblende must be different. Similar cases exist for coexisting anthophyllite-gedrite, in which the differing b axial lengths result in exsolution lamellae nearly parallel to (010) and (120) planes (Robinson et al., 1969; Christie and Olsen, 1974; Gittos et al., 1976; Spear, 1980), and for coexisting glaucophane-cummingtonite, where lamellae of cummingtonite grow in "$28\overline{1}$" and "$2\overline{8}\overline{1}$" orientations (Smelik and Veblen, 1989, 1991).

AMPHIBOLE CHEMISTRY

The complex calcic amphibole assemblages in these rocks have been analyzed using electron microprobe (EMP) and analytical electron microscopy (AEM) techniques. Because the valence state of Fe cannot be determined from these techniques, amphibole compositions were recalculated using a 23 O atom basis, assuming all Fe is Fe^{2+}. Since optical examination of the calcic amphiboles showed them to be a blue-green color in some cases, there is probably considerable Fe^{3+}. The electron microprobe analyses have therefore also been recalculated, normalized to both 15 cations excluding Na, K (15eNK) and 13 cations excluding Ca, Na, and K (13eCNK). Cations were assigned to the various crystallographic sites following the method of Robinson et al. (1982).

Bulk amphibole compositions

Since the exsolution microstructure is so fine scale, microprobe analyses only provide bulk amphibole compo-
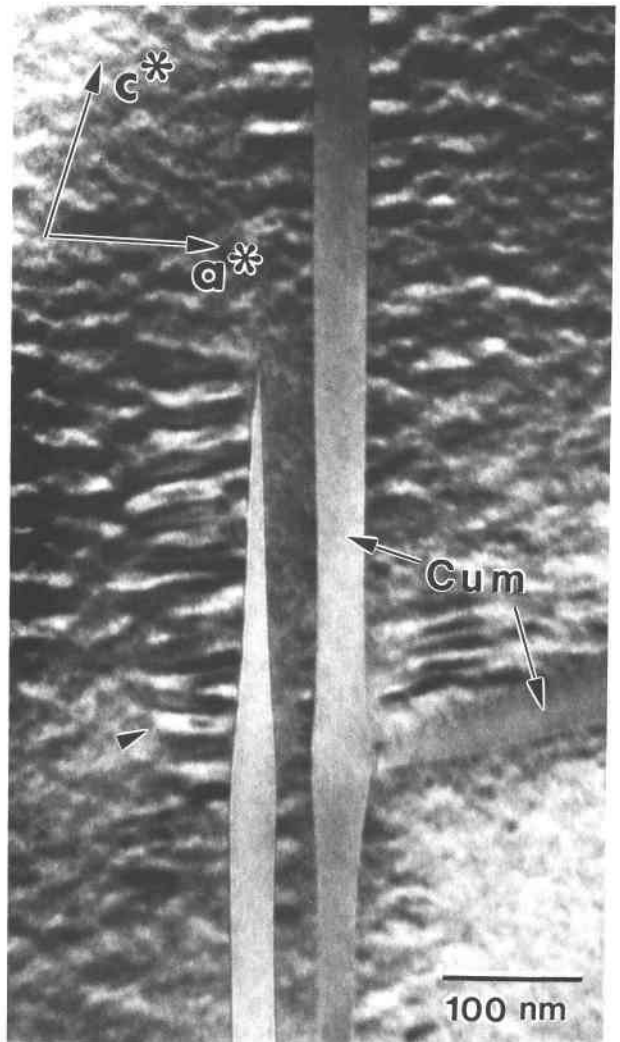

Fig. 5. Bright field TEM image showing coarsening (arrow) of tweed exsolution at "100" cummingtonite lamellar interfaces. The electron beam is parallel to **b**. Coarsening may have been enhanced because of the strain energy at these interfaces, or these may be sites of heterogeneous nucleation.

sitions. Representative EMP analyses of the amphiboles based on the all-Fe^{2+} assumption are presented in Table 2. These analyses were taken along traverses across large, compositionally zoned porphyroclasts and associated equant subgrains. Note that most of these analyses show a slight excess of cations in the M4 site, further evidence of Fe^{3+}. The 13eCNK recalculations of the analyses shown in Table 2 indicate calculated Fe^{3+} contents ranging from 0.561 to 0.950, whereas the estimates for Fe^{3+} for the 15eNK method range from 0.142 to 0.380. Tables 3 and 4, showing these results, are on deposit.[1] Bulk amphibole

[1] Copies of Tables 3 and 4 may be ordered as Document AM-91-463 from the Business Office, Mineralogical Society of America, 1130 Seventeenth Street NW, Suite 330, Washington, DC 20036. Please remit $5.00 in advance for the microfiche.
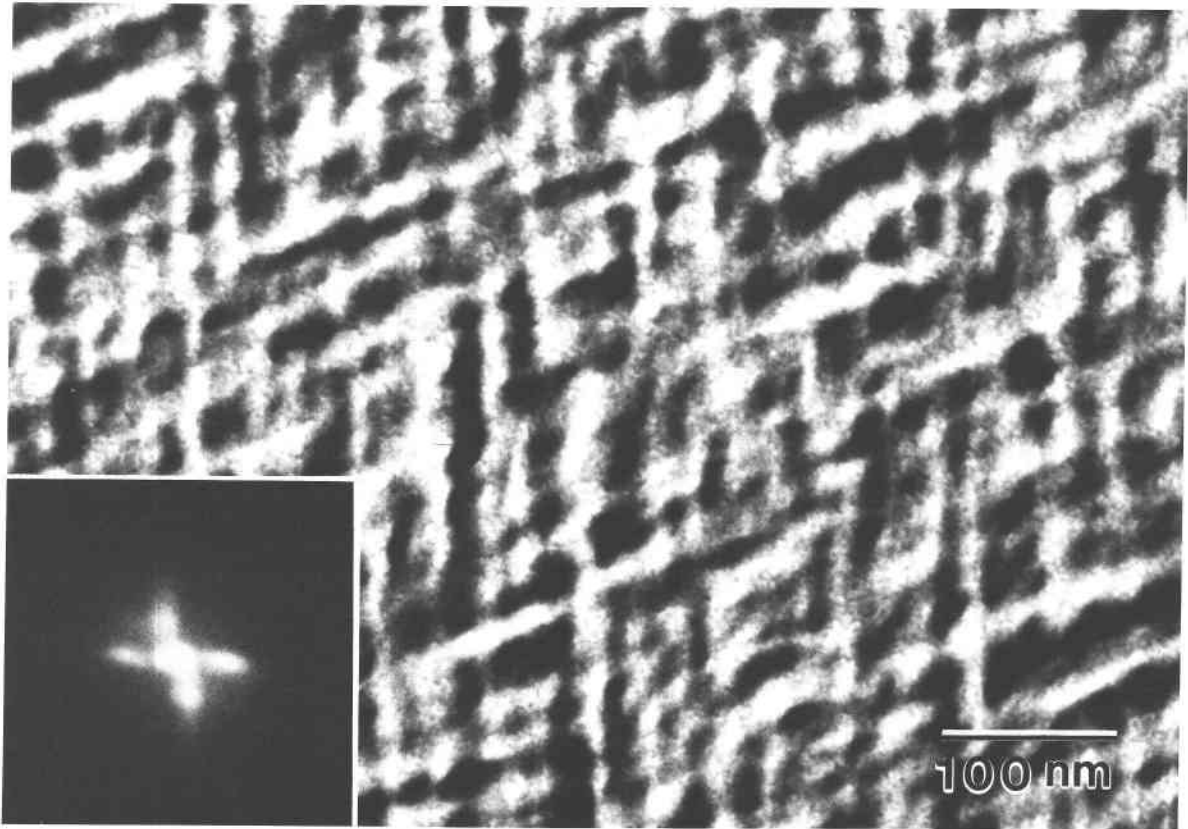
Fig. 6. TEM image of coarse tweed texture tilted so that both sets of compositional modulations are in strong diffracting orientation. The inset shows a greatly enlarged diffraction spot surrounded by satellite reflections, indicating the periodic nature of the microstructure. This observation is suggestive of spinodal decomposition.

analyses were also obtained using AEM (Table 5), employing two methods. In areas showing a very fine tweed microstructure, the EDS spectrum was obtained using an astigmatic, diffuse beam approximately 50×100 nm in dimensions. In coarse tweed areas, this broad beam technique was also used, but the beam was continuously moved over the area while the spectrum was obtained.

Note that the bulk amphibole compositions, presented in both tables, span a large portion of the calcic amphibole series, from actinolite ($Al_{tot} = 0.559$) to magnesio-hornblende ($Al_{tot} = 2.587$) (nomenclature of Leake, 1978). The Na content for these amphiboles varies much less in the EMP analyses (Table 2) than in the AEM analyses (Table 5). This is probably because of the inherently poorer qual-

TABLE 2. Representative EMP analyses from calcic amphiboles

Sample no. Analysis no.		62B tr4.8	62B tr4.12	62B tr4.25	62B tr4.24	62B tr4.5	62B tr4.3	62B tr4.4	62B tr4.1
Tetrahedral sites	Si	6.315	6.502	7.644	7.552	7.105	6.962	6.927	7.113
	Al	1.685	1.498	0.356	0.448	0.895	1.038	1.073	0.887
	Σ T site	8.000	8.000	8.000	8.000	8.000	8.000	8.000	8.000
M(1, 2, 3)	Al	0.902	0.860	0.203	0.200	0.355	0.494	0.517	0.469
	Ti	0.064	0.046	0.014	0.028	0.051	0.075	0.071	0.052
	Mg	1.890	1.990	3.244	3.195	2.766	2.562	2.558	2.807
	Fe^{2+}	2.144	2.104	1.538	1.578	1.828	1.870	1.854	1.672
	Σ M(1, 2, 3)	5.000	5.000	4.999	5.001	5.000	5.001	5.000	5.000
M(4)	Ca	1.949	1.928	1.884	1.861	1.890	1.811	1.813	1.820
	Fe^{2+}	0.165	0.126	0.135	0.165	0.168	0.202	0.247	0.205
	Mn	0.011	0.038	0.026	0.037	0.048	0.034	0.028	0.036
	Σ M(4)	2.125	2.092	2.045	2.063	2.106	2.046	2.088	2.061
A site	Na	0.324	0.301	0.024	0.060	0.180	0.236	0.161	0.148
	K	0.081	0.062	0.011	0.006	0.045	0.065	0.080	0.044
	Σ A site	0.405	0.363	0.035	0.066	0.225	0.301	0.241	0.191
$Fe^{2+}/(Fe^{2+} + Mg)$		0.550	0.528	0.340	0.353	0.419	0.447	0.451	0.401

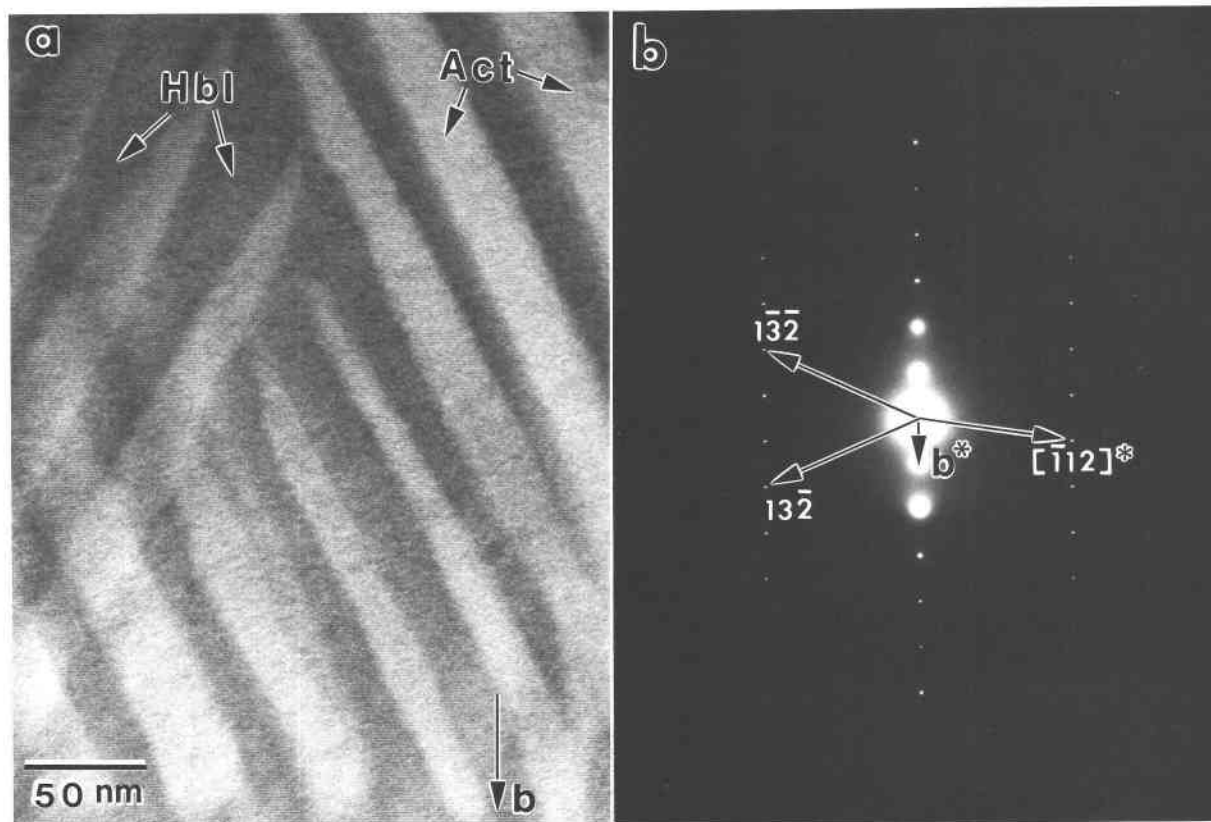Note: Amphibole formula based on normalization to 23 O atoms and assuming all FeO.

Fig. 7. Orientation of actinolite-hornblende exsolution lamellae. (a) TEM image viewed down [201] of an anomalously coarse area. Note that the lamellar interfaces are relatively straight and sharp. (b) Corresponding SAED pattern of the [201] zone, showing the $\mathbf{b}^*$-$[\bar{1}12]^*$ reciprocal lattice plane. The $1\bar{3}2$ and $13\bar{2}$ reflections have been labeled in the diffraction pattern. Note that the $[1\bar{3}2]^*$ reciprocal lattice vector is nearly perpendicular to the set of lamellae running northeast, and the $[13\bar{2}]^*$ vector is nearly normal to the northwest set of lamellae. Since these lamellae may be slightly tilted and the angles are not exactly 90°, these are only approximate orientations and should be designated "$13\bar{2}$" and "$1\bar{3}2$." The symmetrical relationship between the orientations can also be seen.

TABLE 5. Representative bulk AEM analyses for exsolved calcic amphiboles

Sample no. Spectrum no. Exsolution texture		62F 2F25B Coarse	62B 62B19B Coarse	62B 62B20B Coarse	62F 2F56B Fine	62F 2F58B Medium	62F 2F28B Fine	62F 2F48B Fine	62F 2F23B Fine
Tetrahedral sites	Si	7.080	6.979	7.235	7.392	7.216	6.823	7.384	6.684
	Al	0.920	1.021	0.765	0.608	0.784	1.177	0.616	1.316
	Σ T site	8.000	8.000	8.000	8.000	8.000	8.000	8.000	8.000
M(1, 2, 3)	Al	0.444	0.733	0.788	0.237	0.335	0.701	0.254	0.654
	Ti	0.027	0.012	0.014	0.009	0.035	0.046	0.025	0.051
	Mg	2.760	2.701	2.478	2.975	2.930	2.083	2.853	2.213
	Fe^{2+}	1.768	1.555	1.720	1.779	1.700	2.169	1.868	2.082
	Σ M(1, 2, 3)	4.999	5.001	5.000	5.000	5.000	4.999	5.000	5.000
M(4)	Ca	1.818	1.589	1.754	1.900	1.711	1.927	1.881	1.832
	Na	0.068	0.210	0.065	0.000	0.175	0.016	0.075	0.000
	Fe^{2+}	0.103	0.192	0.168	0.085	0.097	0.027	0.014	0.167
	Mn	0.011	0.010	0.013	0.040	0.017	0.031	0.029	0.037
	Σ M(4)	2.000	2.001	2.000	2.025	2.000	2.001	1.999	2.036
A site	Na	0.431	0.422	0.014	0.294	0.487	0.320	0.356	0.400
	K	0.059	0.053	0.000	0.009	0.068	0.080	0.031	0.090
	Σ A site	0.490	0.475	0.014	0.303	0.555	0.400	0.387	0.490
$Fe^{2+}/(Fe^{2+} + Mg)$		0.404	0.393	0.432	0.385	0.380	0.513	0.397	0.504

Note: Amphibole formula based on normalization to 23 O atoms and assuming all FeO.

ity of AEM analyses compared to EMP analyses, especially for Na, resulting from Na loss in the beam and low detection efficiency. In addition, where concentrations of elements are small (e.g., Na and K in these samples), the actual concentrations are subject to analytical errors because of poor counting statistics at low count rates. Also, they may be additionally enhanced or reduced as a result of minor errors in the background subtraction method applied to the raw spectra (Twist algorithm of Aden and Buseck, 1979). Analytical errors are compounded when analyzing very small precipitates because the overall count rates are much lower (see discussion of AEM procedures in Livi and Veblen, 1987, Appendix 2, for more information).

The transition from tremolite-actinolite to hornblende is dominated by three substitution mechanisms within the basic tremolite structure (neglecting Fe^{3+}). These are the edenite substitution $(Na,K)^A,^{[4]}Al \leftrightarrow \square^A,^{[4]}Si$, the tschermakite substitution $^{[6]}Al,^{[4]}Al \leftrightarrow ^{[6]}Mg,^{[4]}Si$, and the $Fe^{2+} \leftrightarrow Mg$ exchange (Robinson et al., 1982). Thompson (1982) has presented an algebraic method by which any mineral composition can be expressed vectorially in terms of a single additive component and a series of exchange components. Viewing composition space in this way allows a quantitative assessment of the exchange vectors for the two amphiboles. The bulk amphibole compositions given in Tables 2 and 5 have been recast in this manner using tremolite, $Ca_2Mg_5Si_8O_{22}(OH)_2$, as the additive component and the following substitutions: $FeMg_{-1}$, $MnMg_{-1}$, $NaAlCa_{-1}Mg_{-1}$ (glaucophane), $Al_2Mg_{-1}Si_{-1}$ (tschermakite), $NaAlSi_{-1}$ (sodium edenite), $TiAl_2Mg_{-1}Si_{-2}$ (titanium tschermakite), $MgCa_{-1}$ (cummingtonite), and $KAlSi_{-1}$ (potassium edenite). As expected, the only significant exchange components between these calcic amphiboles are the tschermakite exchange, edenite exchange, and the Fe-Mg exchange.

The bulk amphibole compositions are plotted in terms of the edenite and tschermakite substitutions in Figure 8. Note that there is considerable scatter in the AEM data, whereas the EMP data form a much tighter trend. Part of this scatter, especially the variation in edenite component, may result from the inherent problems in analyzing Na in the TEM, as discussed above. Despite this problem, a substantial range in bulk compositions is clearly present in these samples. All the calcic amphiboles have both edenite and tschermakite components. Note from Figure 8 that there is a bimodal distribution of bulk AEM analyses from the fine tweed areas (see, e.g., Fig. 2d), whereas the compositions of the more coarsely exsolved regions (see, e.g., Figs. 2a and 6) fall between them. This suggests that the range of bulk compositions spans the actinolite-hornblende solvus, with fine-scale tweed exsolution occurring on the Al-rich and Al-poor limbs and the coarser textures developing from bulk compositions in the middle. This systematic textural variation probably occurs because the intermediate compositions intersect the solvus at higher temperatures and therefore coarsen more than the Al-rich and Al-poor compositions on the limbs
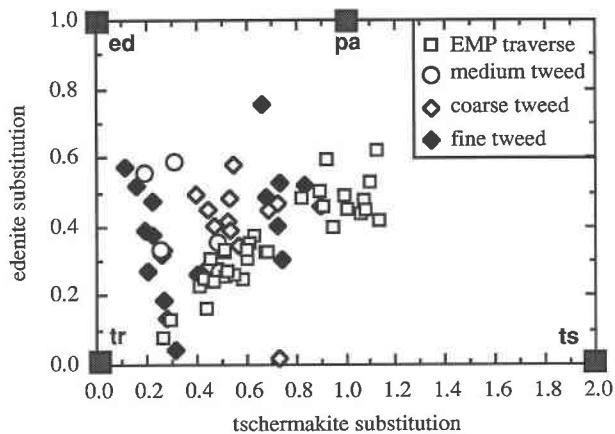

Fig. 8. Plot of EMP and AEM bulk amphibole compositions from porphyroclasts and subgrains in terms of tschermakite and edenite substitution vectors. These compositions cover much of the calcic amphibole series and span the actinolite-hornblende solvus. The scatter in the edenite component for the AEM analyses probably results from analytical errors for Na, as discussed in the text. End-members are tr = tremolite, ed = edenite, pa = pargasite, ts = tschermakite.

of the solvus. The Thompson method also reveals that as bulk compositions change from actinolite to hornblende, there is a steady increase in $FeMg_{-1}$ [i.e., an increase in $Fe^{2+}/(Fe^{2+} + Mg)$]. This is consistent with previous reports of coexisting actinolite-hornblende (Robinson et al., 1982, Fig. 32, p. 72–73).

Composition of actinolite and hornblende lamellae

EDS analysis of the individual lamellae was hindered by several factors including the small size of the lamellae, the diffuse interfaces between the two amphiboles, and tilting of the exsolution lamellae with respect to the beam when orienting the specimen goniometer for optimum take-off angle toward the detector. Despite these problems, it was evident from the X-ray spectra that there is significant partitioning of Al between the two sets of lamellae in the tweed areas. Using a very fine probe (≈ 10–20 nm), analyses of individual lamellae in coarse tweed areas like those shown in Figure 2a were obtained. One set of lamellae showed Al_{tot} ranging from 1.16 atoms per formula unit (pfu) to 1.49 atoms pfu, whereas the other set of lamellae has Al_{tot} ranging from 1.64 atoms pfu to 2.06 atoms pfu. Although partitioning of Al is evident in the tweed areas, these analyses do not represent the compositions of pure phases because of contributions to analyses from neighboring lamellae due to their small size and tilted orientations.

Several anomalously coarse areas were found that contained large lamellae (30–40 nm thick) with relatively sharp interfaces (Figs. 7 and 9). These areas were oriented so that tilting the specimen for analysis fortuitously brought at least one set of lamellae into a nearly edge-on orientation. Representative AEM analyses of these lamellae are
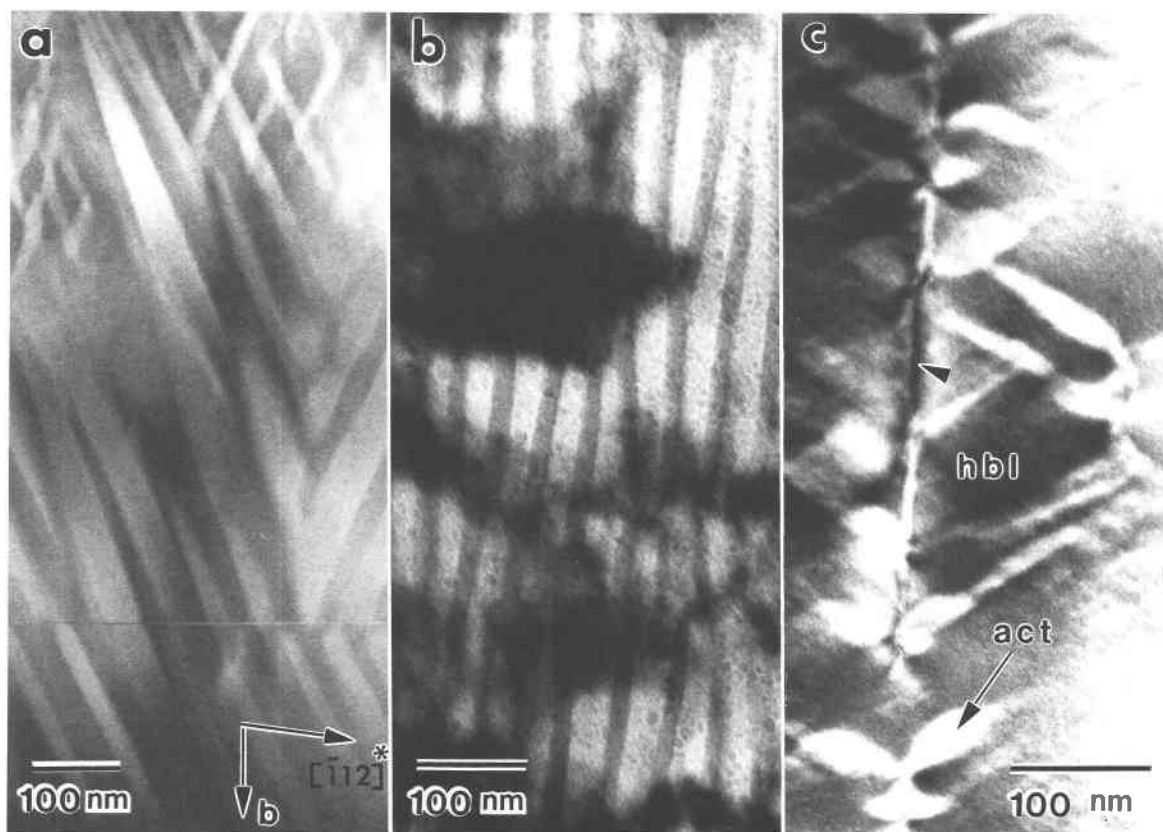
Fig. 9. Bright field TEM images of anomalously coarse exsolution textures where AEM analyses of individual lamellae were obtained. (a) Coarse exsolution viewed down [201] zone. This is a lower magnification image of the area shown in Figure 7a. The sharp horizontal feature near the bottom is a chain-width error. (b) In this nonzone-axis orientation one set of lamellae, running north to south, has short dimensions nearly parallel to the plane of the photo. The lamellae with dark contrast are hornblende, and the light lamellae are actinolite. The other set of lamellae is tilted to a high angle and appears as dark blotches in the image. (c) This image shows coarse actinolite lamellae growing at a subgrain boundary (arrow). These coarse lamellae probably formed by heterogeneous nucleation and growth.

TABLE 6. Representative AEM analyses for actinolite lamellae

Sample no. Spectrum no.		62F 2F88B	62F 2F72B	62F 2F74B	62F 2F75B	62B 2B61B	62B 2B67B	62F 2F81B	62F 2F83B
Tetrahedral sites	Si	7.513	7.670	7.496	7.637	7.523	7.660	7.733	7.703
	Al	0.487	0.330	0.504	0.363	0.477	0.340	0.267	0.297
	Σ T site	8.000	8.000	8.000	8.000	8.000	8.000	8.000	8.000
M(1, 2, 3)	Al	0.366	0.522	0.395	0.427	0.228	0.208	0.502	0.467
	Ti	0.000	0.010	0.014	0.023	0.052	0.021	0.004	0.000
	Mg	3.346	2.794	3.003	2.831	3.245	3.256	3.063	3.248
	Fe^{2+}	1.287	1.671	1.589	1.716	1.474	1.514	1.431	1.285
	Mn	0.000	0.003	0.000	0.003	0.000	0.000	0.000	0.000
	Σ M(1, 2, 3)	4.999	5.000	5.001	5.000	4.999	4.999	5.000	5.000
M(4)	Ca	1.537	1.781	1.791	1.785	1.729	1.698	1.511	1.527
	Na	0.257	0.134	0.120	0.182	0.009	0.029	0.419	0.384
	Fe^{2+}	0.202	0.000	0.075	0.000	0.217	0.255	0.042	0.068
	Mn	0.004	0.036	0.013	0.033	0.044	0.018	0.027	0.021
	Σ M(4)	2.000	1.951	1.999	2.000	1.999	2.000	1.999	2.000
A site	Na	0.347	0.000	0.168	0.023	0.144	0.105	0.136	0.188
	K	0.030	0.022	0.034	0.049	0.009	0.013	0.039	0.027
	Σ A site	0.377	0.022	0.202	0.072	0.153	0.118	0.175	0.215
$Fe^{2+}/(Fe^{2+} + Mg)$		0.308	0.374	0.357	0.377	0.343	0.352	0.325	0.294

Note: Amphibole formula based on normalization to 23 O atoms and assuming all FeO.

TABLE 7. Representative AEM analyses for hornblende lamellae

Sample no. Spectrum no.		62B 2B79B	62B 2B80B	62F 2F95B	62F 2F78B	62F 2F82B	62F 2F85B	62B 2B78B	62F 2F84B
Tetrahedral sites	Si	6.507	6.497	6.470	6.607	6.531	6.392	6.586	6.595
	Al	1.493	1.503	1.530	1.393	1.469	1.608	1.414	1.405
	Σ T site	8.000	8.000	8.000	8.000	8.000	8.000	8.000	8.000
M(1, 2, 3)	Al	0.655	0.706	0.837	0.751	0.963	0.922	0.764	1.155
	Ti	0.064	0.088	0.048	0.041	0.030	0.022	0.056	0.033
	Mg	1.904	1.742	1.718	1.863	1.564	1.685	1.740	1.335
	Fe^{2+}	2.377	2.463	2.397	2.345	2.443	2.371	2.440	2.477
	Σ M(1, 2, 3)	5.000	4.999	5.000	5.000	5.000	5.000	5.000	5.000
M(4)	Ca	1.953	1.936	1.804	1.980	1.770	1.726	1.947	1.824
	Na	0.000	0.003	0.000	0.000	0.015	0.000	0.000	0.049
	Fe^{2+}	0.008	0.030	0.219	0.040	0.185	0.283	0.098	0.098
	Mn	0.040	0.030	0.039	0.026	0.030	0.018	0.035	0.029
	Σ M(4)	2.001	1.999	2.063	2.046	2.000	2.027	2.080	2.000
A site	Na	0.563	0.455	0.271	0.340	0.392	0.486	0.255	0.099
	K	0.146	0.169	0.201	0.128	0.070	0.102	0.125	0.133
	Σ A site	0.709	0.624	0.471	0.468	0.462	0.588	0.380	0.233
$Fe^{2+}/(Fe^{2+} + Mg)$		0.556	0.589	0.604	0.561	0.627	0.612	0.593	0.659

Note: Amphibole formula based on normalization to 23 O atoms and assuming all FeO.

presented in Tables 6 and 7 and plotted in Figure 10. In general, the actinolite lamellae have higher Si, lower Al, lower $Fe^{2+}/(Fe^{2+} + Mg)$ ratio, and lower apparent A-site occupancy than the hornblende lamellae. In addition, Na appears to be redistributed with slightly more Na^{M4} in the actinolite and more Na^A in the hornblende. With regard to the A-site occupancies, it should be reemphasized that the low accuracy of AEM analyses (compared to EMP), especially for Na, leads to quite variable A-site contents for amphibole formulas. Furthermore, the chosen renormalization scheme maximizes the numbers of cations pfu, and since it is likely that these amphiboles contain some Fe^{3+}, the A-site contents shown may be overestimated. The apparent redistribution of Na is probably an artifact of the AEM process, the difference in Fe contents, and the recalculation scheme. The average $Fe^{2+}/(Fe^{2+} + Mg)$ ratios for the exsolved phases are 0.349(52) for the actinolite and 0.588(92) for the hornblende. The miscibility gap defined by these compositional differences is shown graphically in Figure 10. Figure 10a is a plot of Al_{tot} vs. $Fe^{2+}/(Fe^{2+} + Mg)$ for 20 actinolite and 21 hornblende AEM analyses (including those in Tables 6 and 7). Figure 10b shows the gap in terms of calculated A-site occupancy vs. [4]Al. Al_{tot} is plotted against [4]Al in Figure 10c. In each plot, the miscibility gap is well defined. The large circles connected by tie lines in Figure 10 show the positions of the average compositions of actinolite and hornblende lamellae determined by AEM. The average of the 20 best actinolite analyses is $K_{0.03}Na_{0.12}(Na_{0.18}Ca_{1.71}Fe_{0.08}Mn_{0.03})$-$(Fe_{1.55}Mg_{3.05}Al_{0.38}Ti_{0.02})[Al_{0.38}Si_{7.62}]O_{22}(OH)_2$. Averaging of the 21 best hornblende analyses yielded $K_{0.14}Na_{0.36}(Ca_{1.88}Fe_{0.16}Mn_{0.02})(Fe_{2.4}Mg_{1.8}Al_{0.76}Ti_{0.05})[Al_{1.48}Si_{6.52}]O_{22}(OH)_2$.

As was mentioned earlier, the calcic amphibole series can be described in terms of three primary substitution mechanisms: the edenite and tschermakite substitutions and the Fe ↔ Mg exchange. By expressing the above compositions vectorially using the Thompson (1982) method, we can determine the magnitude of these substitutions

resulting from the exsolution (Table 8). Table 8 shows the vector representation of the average lamellar compositions (shown above) and the bulk amphibole composition averaged from 24 AEM analyses of the coarse tweed areas; this represents the amphibole composition before the onset of exsolution. From these results, it is clear that both the edenite and tschermakite substitutions operated during exsolution, with the tschermakite exchange being dominant. As mentioned above, the calculated A-site contents are to be regarded with caution for several reasons, and since the A-site contents are directly tied to the amount of edenite exchange, the magnitude of this vector should also be accepted with caution. It seems likely that the edenite component may be overestimated. Note that the method assuming that all Fe is Fe^{2+} results in some cummingtonite component in both the actinolite and hornblende, with small amounts of Fe^{2+} assigned to M4.

OPTIMAL PHASE BOUNDARY CALCULATIONS

It was shown earlier that the actinolite and hornblende exsolution lamellae are oriented parallel to irrational planes

TABLE 8. Vector representatation of average calcic amphibole compositions (from AEM of individual lamellae)

| Mineral		Bulk coarse tweed	Actino- lite lamellae	Hornblende lamellae
No. of analyses		(24)	(20)	(21)
Vector components				
Additive	tremolite	1.000	1.000	1.000
Exchange	$FeMg_{-1}$	1.970	1.634	2.546
Exchange	$MnMg_{-1}$	0.026	0.026	0.027
Glaucophane	$NaAlCa_{-1}Mg_{-1}$	0.022	0.018	−0.060
Tschermakite	$Al_2Mg_{-1}Si_{-1}$	0.516	0.195	0.819
Sodium edenite	$NaAlSi_{-1}$	0.368	0.124	0.425
Titanium tschermakite	$TiAl_2Mg_{-1}Si_{-2}$	0.035	0.017	0.053
Cummingtonite	$MgCa_{-1}$	0.086	0.109	0.182
Potassium edenite	$KAlSi_{-1}$	0.052	0.025	0.134
Total edenite		0.420	0.150	0.559
Total tschermakite		0.551	0.212	0.872
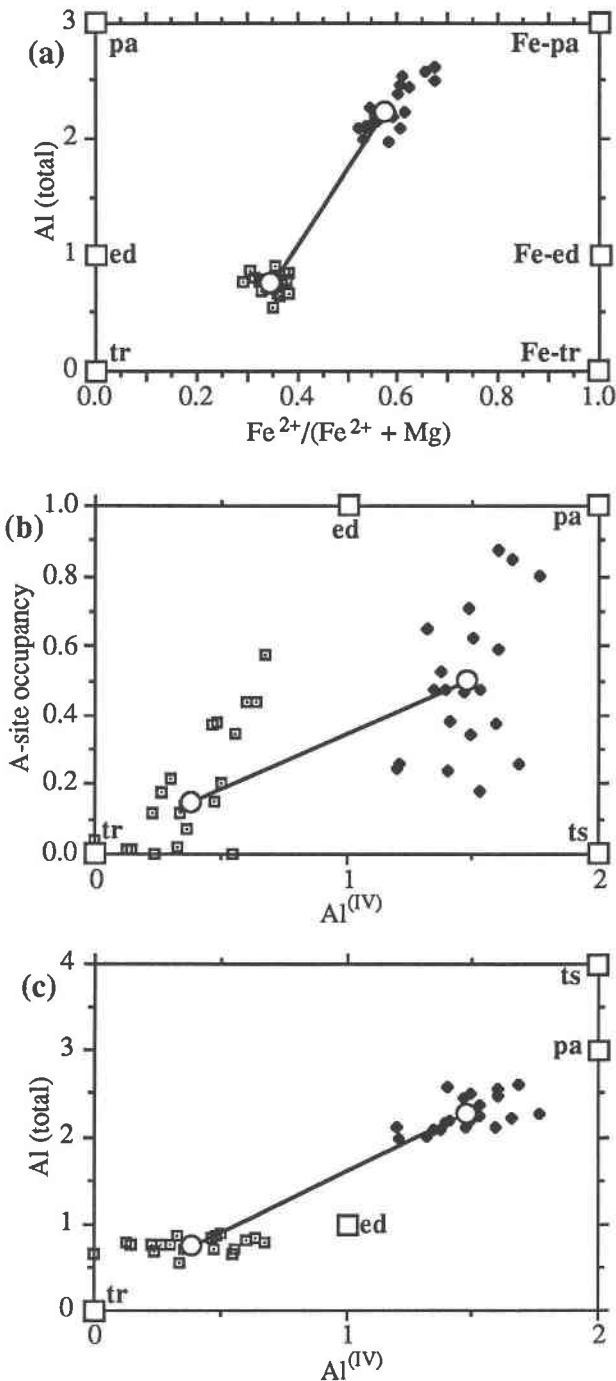
Fig. 10. Plots of AEM analyses of individual actinolite and hornblende lamellae, showing the miscibility gap. Open squares are for actinolite and filled diamonds are for hornblende. The open circles connected by a tie line represent the average compositions. (a) Plot of total Al vs. $Fe^{2+}/(Fe^{2+} + Mg)$. (b) Plot of calculated A-site occupancy vs. [4]Al. (c) Plot of Al_{tot} vs. [4]Al. Abbreviations for end-members as in Figure 8.

close to $(13\bar{2})$ and $(1\bar{3}\bar{2})$. Furthermore, TEM images and SAED patterns suggest that the tweed exsolution microstructure may have formed by spinodal decomposition.

During exsolution processes, the overall change in free energy accompanying precipitation of a second phase is generally expressed as $\Delta G_{tot} = \Delta G_{volume} + \Delta G_{surface} + \Delta G_{strain}$. For all coherent exsolution processes, the strain energy associated with the volume difference between the two phases, ΔG_{strain}, contributes significantly to the activation energy barrier and, more importantly, controls the orientation of compositional modulations and nucleated exsolution lamellae (Cahn, 1961, 1962, 1968; Willaime and Brown, 1974; Robin, 1974; Champness and Lorimer, 1976; Fleet, 1982). Several studies have suggested that the minimization of the interfacial strain energy is the dominant factor controlling the orientation of coherent precipitates (Bollman and Nissen, 1968; Robinson et al., 1971; Willaime and Brown, 1974; Robin, 1974, 1977; Jaffe et al., 1975; Robinson et al., 1977; Fleet et al., 1980; Fleet, 1981, 1982, 1984, 1986; Fleet and Arima, 1985; Smelik and Veblen, 1991).

To test whether the observed lamellar orientations represent optimal phase boundaries along which ΔG_{strain} is minimized, a series of three-dimensional optimal phase boundary calculations were performed for coherently intergrown actinolite-hornblende. The calculations were done using the three-dimensional lattice-fitting program (EPLAG) of Fleet (1982, 1984). This version of EPLAG calculates only the area misfit between normalized equivalent (hkl) planes in the two related lattices and makes no quantitative estimate of elastic strain energy. The area strain was calculated at grid points on a hemisphere about the **b** axis using a grid interval of 5°. Each grid point corresponds to a stereographic pole of an interatomic plane, (hkl), and is described in terms of the spherical coordinates D and E, where D is a counterclockwise rotation about **b** and E is a clockwise rotation about an axis normal to **b** (see Fleet, 1982, for details of the three-dimensional theory). The results are displayed on a stereographic projection down **b,** the equatorial plane being the **a*-c*** reciprocal lattice plane. It is assumed that the calculated orientation showing the minimum area strain between the two normalized equivalent planes corresponds to the minimum value of ΔG_{strain}. This assumption is strictly true only for elastically isotropic structures; nonetheless, such lattice misfit calculations have successfully reproduced exsolution orientations in a number of silicate systems (see above references).

The EPLAG calculations make use of unstrained lattice parameters for the two phases. Since SAED patterns do not provide lattice parameter information of the necessary high accuracy and because lattice parameters determined from coherently exsolved areas are inevitably strained, there was no direct way to determine unstrained parameters. Lattice parameters for the calculations were therefore arrived at using a combination of published data and AEM data.

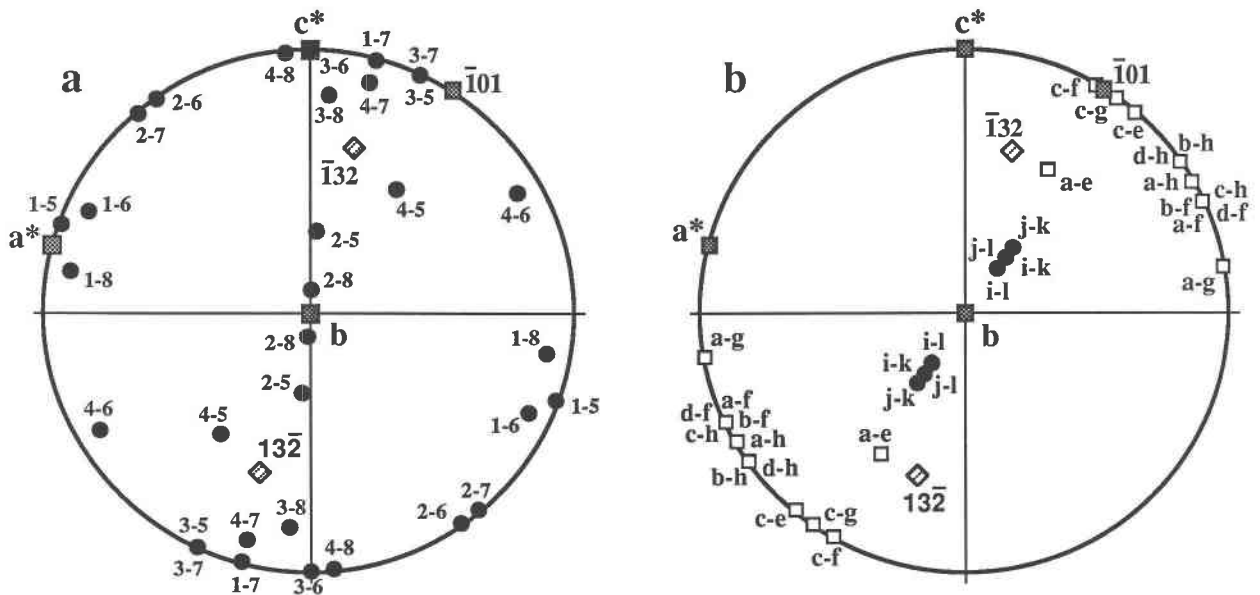The most obvious way to find suitable unstrained lattice

Fig. 11. Stereographic projections down **b** showing results from EPLAG calculations for intergrown actinolite-hornblende. Poles for (001), (010), (100), and ($\bar{1}$01) are shown as stippled boxes. The observed orientations, "13$\bar{2}$" and "$\bar{1}$32," are shown as diamonds. (a) Numbered filled circles are poles to optimal phase boundaries calculated using literature unit cells shown in Table 9 (see cells 1 through 8). Actinolite-hornblende pairs are labeled on the stereogram. Note that pairs 3-8, 4-5, and 4-7 are fairly near the observed orientation. (b) Open squares are poles to optimal phase boundaries calculated using the model unit-cell parameters calculated from the equations of Wenk (1971) (see unit cells a through h in Table 9). Actinolite-hornblende pairs are labeled. Note that the small differences in the *b*-axis magnitudes between most of these pairs lead to optimal phase boundaries in the [010] zone. Pair a-e plots about 12° from the observed orientation. Filled circles are for model unit cells determined using the curve of Ernst (1968) and averaged literature values (unit cells i through l in Table 9). Actinolite-hornblende pairs are labeled.

parameters is to use published unit-cell data for actinolite and hornblende having similar compositions to the actinolite and the hornblende described here. A thorough search of the literature revealed no studies describing actinolite or hornblende having exactly the same compositions, but many gave compositions (with unit-cell information) that were reasonably close to our amphiboles. Another problem to consider, as indicated by Hawthorne (1983 and references therein), is that cation ordering in the calcic amphiboles is exceedingly complex, so even if matching compositions were found, different ordering schemes could result in different unit cells. Despite this, 13 actinolite unit cells [Zussman, 1955, 1959; Ross et al., 1969 (2); Mitchell et al., 1971; Wenk, 1971 (4); Litvin et al., 1972a; Brady, 1974 (2); Cameron, 1975] and 32 hornblende unit cells [Raychaudhuri, 1964 (3); Binns, 1965 (4); Dodge et al., 1968 (2); Papike et al., 1969; Wenk, 1971 (10); Litvin et al., 1972a, 1972b (2), 1973 (these unit-cell parameters were taken from the tabulation of Hawthorne, 1983, Appendix B1, amphibole samples 45, 46, 49); Hawthorne and Grundy, 1973; Bocchio et al., 1978 (3); Charles, 1980 (3); Hawthorne et al., 1980] were chosen from the literature. Of these 45 amphiboles, the data for the four actinolite and hornblende samples closest in composition to the present pair were used in the EPLAG calculations.

Parameters for these eight unit cells are given in Table 9. The results of the calculations are shown in Figure 11a. Each amphibole is given a code number in Table 9 so that the various optimal phase boundary (OPB) orientations can be identified for each actinolite-hornblende pair considered. In Figure 11a, the calculated poles are shown by filled circles and the poles for the observed orientations "13$\bar{2}$" and "$\bar{1}$32" are shown as diamonds. (Note that symmetrically related poles "13$\bar{2}$" and "$\bar{1}$32" plot in the lower hemisphere.) From Figure 11a it is clear that there is a wide range of potential OPB orientations with three pairs (3-8, 4-5, and 4-7) coming fairly close to the observed orientations.

As was discussed earlier, the deviation from the common "100" and "$\bar{1}$01" orientations predicted by the exact phase boundary theory of Robinson et al. (1971, 1977) is thought to be caused by differences in the *b* axial lengths of the two amphiboles. In general, the unit-cell edge that differs the most between each pair exerts a strong influence on the OPB orientation. Since the *b* axis is about twice as long as *a* and about four times as long as *c* among clinoamphiboles, the relative difference in the *b* dimension must be significant relative to differences in the other cell dimensions before the predicted lamellar orientation is not a plane containing the *b* axis, i.e., a plane belonging

TABLE 9.   Unit-cell parameters for EPLAG calculations

Reference	Code[*]	a (Å)	b (Å)	c (Å)	β
Parameters from literature					
Actinolite					
Zussman (1955)	1	9.890	18.140	5.310	105.800
Mitchell et al. (1971)	2	9.891	18.200	5.305	104.640
Wenk (1971) (Varzo 6)	3	9.828	18.074	5.285	104.640
Ross et al. (1969) (HJ182-60)	4	9.839	18.114	5.285	104.550
Hornblende					
Wenk (1971) (Mto 798)	5	9.847	18.074	5.318	104.950
Binns (1965) (H37A)	6	9.827	18.081	5.324	104.960
Raychaudhuri (1964) (H-72)[**]	7	9.857	18.088	5.287	105.000
Hawthorne et al. (1980)	8	9.832	18.037	5.302	105.010
Parameters from AEM data and Equations 1 and 2 of Wenk (1971)[†]					
act (1)-(23)	a	9.836	18.102	5.298	104.675
act (1)-(13)	b	9.850	18.116	5.301	104.740
act (2)-(23)	c	9.803	18.063	5.290	104.576
act (2)-(13)	d	9.831	18.094	5.294	104.601
hbld (1)-(23)	e	9.841	18.082	5.323	104.908
hbld (1)-(13)	f	9.836	18.098	5.326	105.025
hbld (2)-(23)	g	9.844	18.068	5.312	105.006
hbld (2)-(13)	h	9.890	18.119	5.319	105.041
Parameters from calculated M2 contents and curve of Ernst (1968) (for b axis)[‡]					
act (23)	i	9.848	18.167	5.295	104.820
act (13)	j	9.848	18.124	5.295	104.820
hbld (23)	k	9.854	18.010	5.310	104.999
hbld (13)	l	9.854	17.946	5.310	104.999

* These code numbers or letters are cited for actinolite-hornblende pairs plotted in Figure 11.
** No value for β was given in this study, only $a \sin \beta$ and $c \sin \beta$; $\beta = 105°$ was used to calculate a and c.
† For these parameters, the first number in parentheses indicates which equation of Wenk (1971) was used; the second number shows the normalization scheme (23 O atoms, all FeO, or 13 cations excl. CNK).
‡ For these parameters, the number in parentheses shows the normalization scheme. The values for a, c, and β were averaged from 13 actinolites and 32 hornblendes from the literature (see text for references).

to the [010] zone with indices ($h0l$). Consider for example pair 3-6, which shows relative differences in unit-cell parameters equal to 0.010, −0.039, and −0.738% for a, b, and c, respectively. The large relative difference in the c dimension gives rise to an (001) OPB orientation. Likewise, pair 2-8 shows relative differences in unit cell parameters equal to 0.597, 0.896, and 0.057% for a, b, and c, respectively, and its OPB is just 5° from (010). The wide range of calculated OPB orientations for intergrown actinolite-hornblende suggests that since the unit-cell parameters of these two minerals are so similar, a range of lamellar orientations may be possible, depending on the exact compositions and unit-cell dimensions of the intergrown pair. Small changes in composition could result in large changes in orientation.

In addition to using published unit-cell parameters, actinolite and hornblende unit-cell parameters were determined in two other ways. Wenk (1971) correlated clinoamphibole lattice parameters with chemical composition using multivariable regression analysis and presented two equations and associated coefficients by which unit-cell parameters can be calculated (Wenk, 1971, Eqs. 1 and 2 and Table 4, p. 349–351). Equation 1 uses the chemical variables Si, Fe^{3+}, Fe^{2+}, and Mg, whereas Equation 2 uses Si, Fe^{3+}, Fe^{2+}, and Ca. Using both equations, the average compositions given above, and renormalized ones using 13eCNK, four actinolite and four hornblende model unit cells were calculated (cells a–h in Table 9). Using estimated values of Fe^{3+} for the calculations resulted in

very small differences in unit-cell parameters (less than 0.15% for the actinolites and less than 0.5% for the hornblendes). The results from EPLAG on combinations of these cells are shown in Figure 11b (empty squares). Note that all the calculated OPB orientations except one (pair a-e) belong to the [010] zone (i.e., poles are 90° from **b**). The OPB for pair a-e plots about 12° from the observed orientation. Several of the OPB orientations (e.g., c-f, c-g, c-e) are very near that of ($\bar{1}01$) and can also be calculated by using the exact phase boundary theory of Robinson et al. (1971, 1977). Only pair a-e shows enough relative difference in the magnitude of b for the pole of the OPB to be tilted up toward **b**.

A third method of obtaining unit-cell parameters utilized data of Colville and coworkers (1966); they investigated a series of synthetic amphibole compositions to assess the effects of various ionic substitutions on unit-cell parameters of clinoamphiboles. Their results indicate that the magnitude of b is most sensitive to compositional changes and is primarily controlled by the occupancy of M4 and M2. They further show that in any given amphibole series with the contents of M4 remaining essentially constant, the magnitude of b is largely dependent on the occupancy of M2. The magnitudes of a and c are also affected but to a much lesser extent (Colville et al., 1966). For our purposes, we constructed a third set of model unit cells by estimating the magnitude of the b axes from the plot of Ernst (1968), summarizing Colville et al.'s work, showing calculated mean ionic radius of cations

occupying M2 vs. observed magnitude of b. For the present actinolite-hornblende pair, the M2 site occupancies were calculated by first assigning all the Al, Fe^{3+}, and Ti^{4+} to M2 (Papike and Clark, 1968; Bancroft and Burns, 1969; and Hawthorne and Grundy, 1973; Hawthorne, 1981, 1983). Since many studies have indicated that Fe-Mg distribution among the M1, M2, and M3 sites of calcic amphiboles is highly variable (see Hawthorne, 1981, Table 24; Hawthorne, 1983, Table 60), the sites were then filled with equal amounts of Fe^{2+} and Mg. The mean ionic radius in M2 was then calculated using the ionic radii of Shannon and Prewitt (1969). Once this was calculated for both the 23-O atom, all-FeO, and 13eCNK compositions, we determined the magnitudes of b from Figure 3a of Ernst (1968). Since a, c, and β are less sensitive to compositional changes (Colville et al., 1966), we averaged these parameters from the 13 actinolite and 32 hornblende unit cells from the literature mentioned above. The final results of this procedure are shown in the lower part of Table 9 (cells i–l). The EPLAG results for combinations of these model unit-cell parameters are also shown in Figure 11b (filled circles). These OPB orientations, like pairs 2-5 and 2-8 in Figure 11a, reflect substantial differences in b of the actinolite and hornblende model unit cells. The magnitudes of these differences probably exceed the actual differences in the b axes magnitudes for the present actinolite-hornblende pair, since the observed orientation is about 30–40° further from (010).

The combined results from Figure 11 lend further support to the idea that the unusual actinolite-hornblende lamellar orientations we observe in our samples are controlled by dimensional misfit between the actinolite and hornblende lattices. The difference in the magnitudes of b is of prime importance in producing an orientation that is not parallel to **b**, similar to the case of cummingtonite lamellae in glaucophane (Smelik and Veblen, 1991) but different from the "100" and "$\bar{1}01$" orientations found in most exsolved clinoamphiboles (Robinson et al., 1982). An additional result suggested by these calculations that cannot be overemphasized is that because the unit cells of actinolite and hornblende are so similar, lamellar orientations may be quite different from sample to sample, or even within samples, and are probably functions of temperature and pressure as well as bulk amphibole composition. Consistent with Brady's (1974) observation, the potential variations in OPB orientations resulting from these factors may partially explain why irregular and patchy intergrowths of actinolite-hornblende are commonly observed (Klein, 1969; Brady, 1974; Choudhuri, 1974; Tagiri, 1977), rather than intergrowths with perfectly planar interfaces.

DISCUSSION

Exsolution mechanisms

The TEM, HRTEM, and AEM results described above suggest at least two stages of exsolution in these complex calcic amphiboles. The first phase of exsolution involved

the formation of "100" and "$\bar{1}01$" cummingtonite lamellae in some grains (Figs. 2c, 5, and 12). Figure 12 shows a network of coarse cummingtonite lamellae in an actinolitic subgrain. Note that very fine tweed actinolite-hornblende exsolution is also visible between these lamellae, with coarsening at the cummingtonite interfaces. Figure 12a shows the cummingtonite lamellae viewed down **b** in an edge-on orientation. Figure 12b shows the same area tilted significantly from **b**. In this orientation, dislocations associated with the tips of the "100" lamellae can be seen (arrows in Fig. 12b). This observation shows that the cummingtonite and host are not coherently intergrown at the lamellar tips and suggests that the cummingtonite may have formed by heterogeneous nucleation and growth. On the other hand, since HRTEM images show that the cummingtonite–calcic amphibole intergrowth is coherent everywhere else along their interfaces, homogeneous nucleation and growth cannot be ruled out, with dislocations forming during subsequent coarsening. Representative AEM analyses of the cummingtonite lamellae are presented in Table 1. The $Fe^{2+}/(Fe^{2+} + Mg)$ ratio ranges from 0.450 to 0.510 with an average of 0.478. These analyses contain significantly more Mn (1.2–2.0 wt% MnO) than the tweed areas, indicating partitioning of Mn into the cummingtonite during the first precipitation event.

Some time after the nucleation and growth of the cummingtonite, exsolution of actinolite and hornblende began. The style of this precipitation event is markedly different from that of the cummingtonite event. The actinolite-hornblende exsolution forms a pervasive fine-scale tweed texture (Figs. 2, 3, and 6) with coherent compositional modulations in two symmetrical orientations, "$13\bar{2}$" and "$1\bar{3}2$." SAED patterns indicate that the microstructure is rather periodic and produces satellite reflections around individual reciprocal lattice nodes. These observations are consistent with spinodal decomposition (Champness and Lorimer, 1976). The wide variations in the degree of coarseness of the tweed texture combined with the range of bulk amphibole compositions (Tables 2 and 5) suggest that these calcic amphiboles span virtually the entire actinolite-hornblende solvus at these P-T-X conditions. It seems likely that bulk compositions of intermediate Al content ($8.5 \leq Al_2O_3 \leq 10.5$ wt%) encountered the coherent spinodal first at some temperature below 450–500 °C (peak metamorphic temperature estimates of Duebendorfer, 1988 and Nyman et al., 1989). As cooling slowly progressed, these areas began to coarsen, while other areas with slightly different Al content ($Al_2O_3 \leq 8.5$ and $Al_2O_3 \geq 10.5$ wt%) became sufficiently undercooled for spinodal decomposition to begin.

Recalling Figures 4 and 5, significant coarsening of the tweed texture was observed at dislocations and cummingtonite lamellar interfaces. These observations may represent selective heterogeneous nucleation and growth at these sites, or coarsening may have been expedited by the high strain energy or enhanced diffusion at these locations. From these textures and the fact that the subgrains
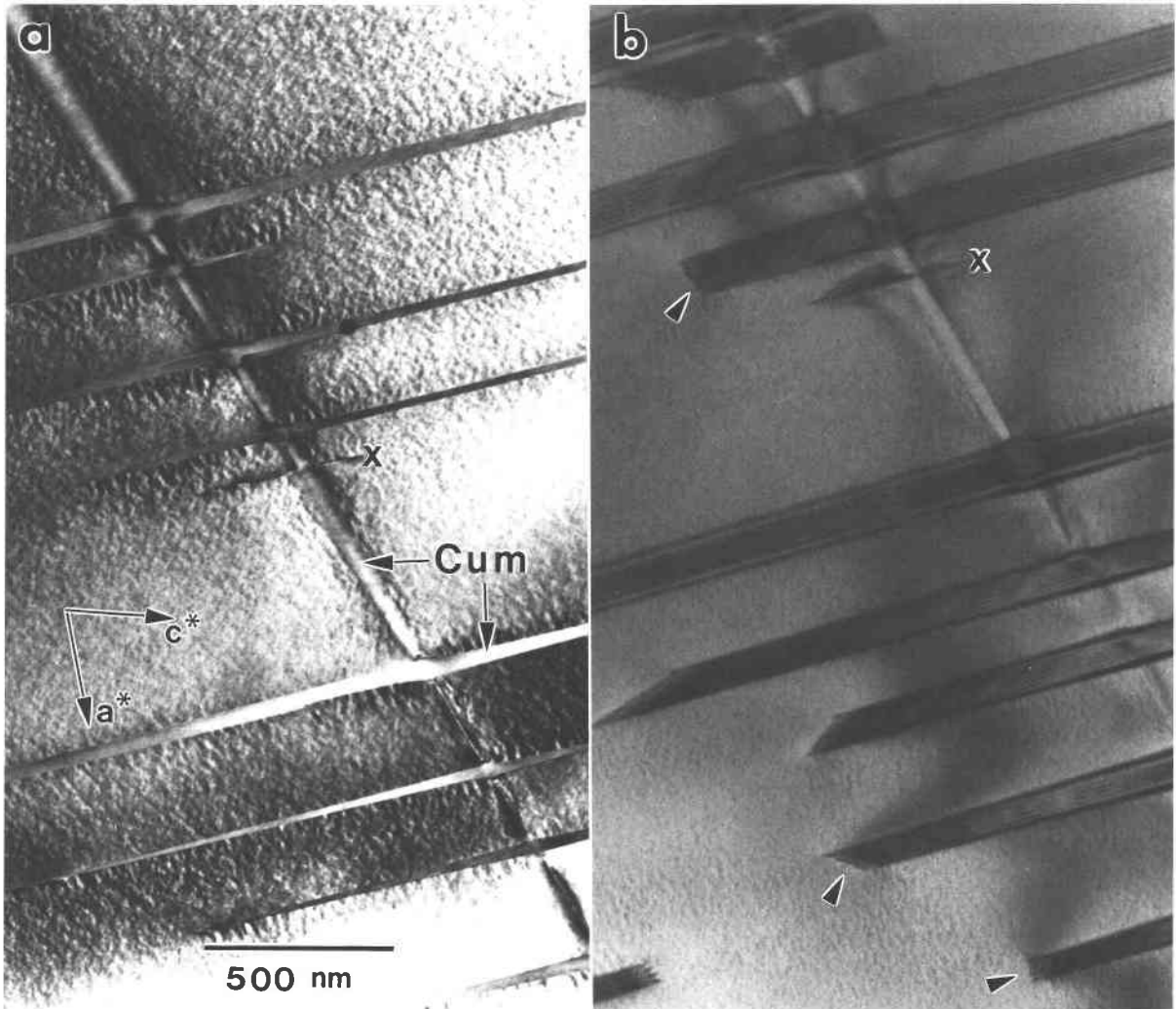
Fig. 12. (a) Bright field TEM image viewed down the **b** axis in a subgrain showing a single "$\bar{1}01$" and several "100" cummingtonite lamellae. Between these large cummingtonite lamellae is pervasive fine-scale actinolite-hornblende exsolution. This texture has coarsened somewhat at cummingtonite lamellar interfaces. (b) Same area in tilted orientation. The "x" marks identical locations in parts **a** and **b**. Note the dislocations at the tips of the "100" cummingtonite lamellae (arrows).

as well as the porphyroclasts are exsolved, it is clear that the formation of the tweed microstructure postdates both the cummingtonite exsolution and some of the deformation in these minerals.

AEM and EMP analyses indicate that these amphiboles are chemically heterogeneous and strongly zoned. Amphibole compositions varied widely not only from grain to grain but within individual grains as well. As noted previously, this zoning is also seen in terms of exsolution textures, as emphasized in Figure 13. This small area (about 3.5 μm^2) within a single grain shows a diverse range of tweed exsolution texture from very fine to fairly coarse. AEM shows that the texture varies with composition, with the very fine areas of Figure 13 having approximately 0.80 Al pfu and the coarser areas having about 1.45 Al pfu. It seems likely that these heterogeneous amphibole assem-

blages do not represent equilibrium crystallization but formed instead during continuous prograde metamorphism, much like the coexisting calcic amphiboles of Graham (1974), Grapes (1975), and Grapes and Graham (1978). The results presented here suggest that this entire heterogeneous assemblage subsequently underwent exsolution during slow cooling from the peak metamorphic temperatures. It seems possible that other heterogeneous calcic amphibole assemblages, like those of Grapes and Graham, may also contain evidence of the actinolite-hornblende miscibility gap at the TEM scale.

The actinolite-hornblende miscibility gap

The results presented here represent the first solid evidence from exsolution for the existence of an actinolite-hornblende miscibility gap. Klein (1969) described "100"
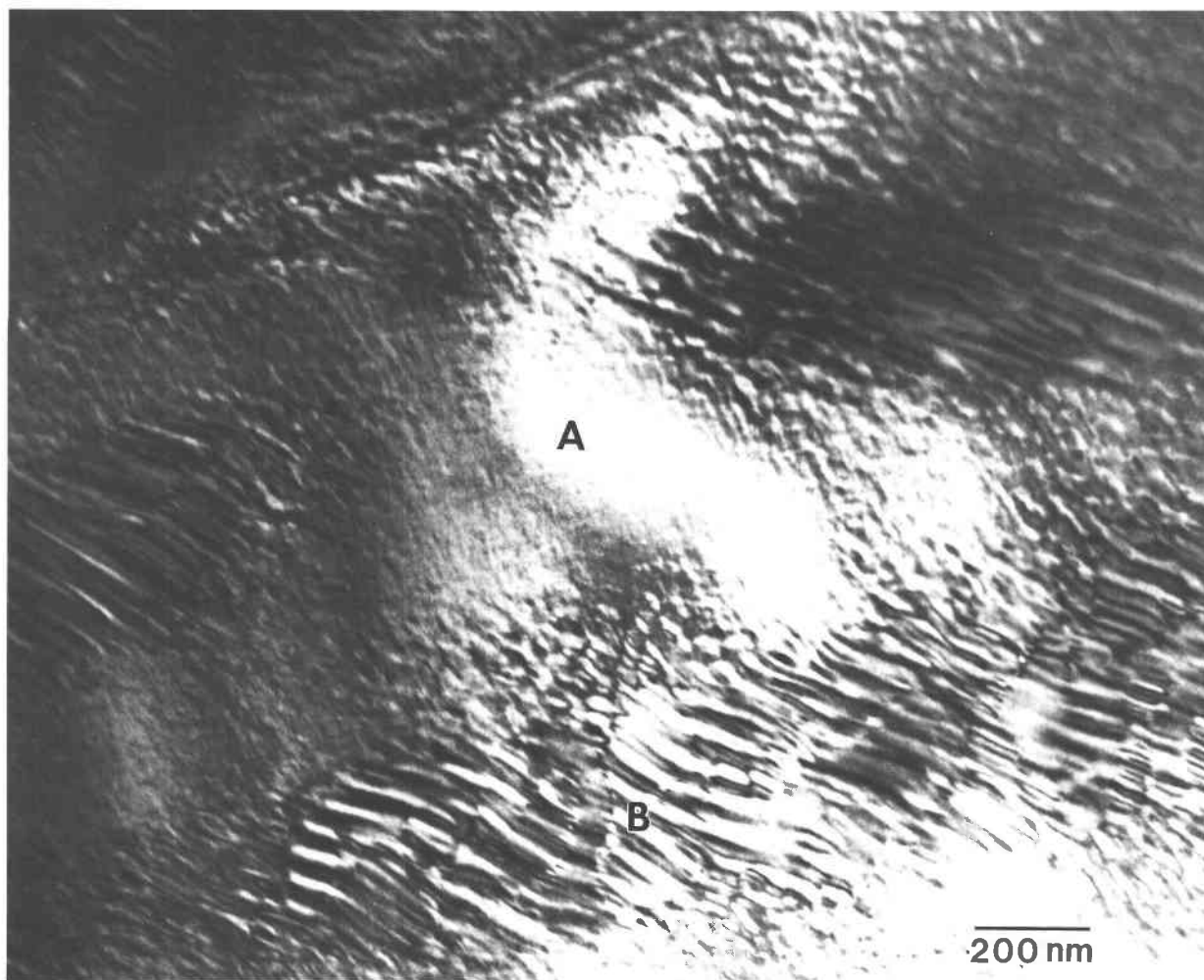
Fig. 13. Bright field TEM image of a small (~3.5 μm²) area showing actinolite-hornblende exsolution ranging from very fine scale tweed (A) to fairly coarse tweed (B). These varying textures formed as a result of compositional zoning in the bulk amphibole. Bulk AEM analyses indicate that the fine scale tweed (A) has approximately 0.80 total Al atoms pfu, whereas the coarse tweed (B) has about 1.45 total Al atoms pfu. Note also that the lamellar interfaces are curved, suggesting a variable orientation.

and "$\bar{1}01$" exsolution lamellae in samples of hornblende coexisting with actinolite from Madagascar and suggested that they might be actinolite. Our results suggest that these lamellae are probably cummingtonite, and any true actinolite-hornblende exsolution would probably occur on a much finer scale, probably directly visible only with electron microscopy. In a study of deformation in calcic amphiboles, Biermann and Van Roermund (1983) noted the presence of a modulated microstructure similar to that described here but did not investigate it in any detail. Similar exsolution phenomena were also observed in calcic amphiboles from mylonites in Norway (Cumbest, personal communication, 1990). It seems possible that exsolution involving actinolite and hornblende may be far more common than previously thought but has gone unobserved because of the fine scale and perhaps unusual orientation of the microstructures.

The actual shape and size of the actinolite-hornblende solvus is undoubtedly dependent on numerous factors including pressure, temperature, and bulk composition. The work of Oba and Yagi (1987) suggests a narrowing of the solvus with increasing Fe, whereas the study of Tagiri (1977) implies the opposite trend. Oba and Yagi suggest that the discrepancy may be due to Fe_2O_3 content, which appears to exert a considerable influence on the extent of the gap. The experimental work of Oba (1980) and Oba and Yagi (1987) on calcic amphibole solutions and studies of thermal stabilities of Fe-rich calcic amphiboles by Ernst (1966) and Gilbert (1966) suggest that the crest of the actinolite-hornblende solvus will be at lower temperatures for Fe-bearing systems than for Mg-rich systems.

As a result of the large number of variables controlling the size and shape of the solvus, comparison of the many

published compositions of coexisting actinolite-hornblende, including the present ones, on two-dimensional diagrams may obscure the true nature of the solvus. The large volume of work pertaining to this problem has led to a good understanding of the general crystal-chemical trends in the actinolite-hornblende system. Contributions from the present paper toward that understanding include the following:

1. The miscibility gap unquestionably does exist under the P-T-X conditions of our samples and involves primarily the operation of three amphibole cation exchanges: edenite, tschermakite, and Fe-Mg exchange. The tschermakite exchange dominates over that of edenite, and the hornblende is significantly richer in Fe than the actinolite, consistent with previous reports.

2. Actinolite-hornblende exsolution is pervasive in these samples, with spinodal decomposition thought to be the primary mechanism of phase separation.

3. The compositional modulations commonly occur in two symmetrical orientations, nearly parallel to $(13\overline{2})$ and $(1\overline{3}2)$ of the $C2/m$ amphibole setting.

4. In coarsened areas, the tweed microstructure is periodic, with satellite reflections appearing in SAED patterns, indicating a 25- to 35-nm periodicity.

5. Optimal phase boundary calculations for intergrown actinolite-hornblende indicate that "$13\overline{2}$" and "$1\overline{3}2$" probably do represent minimum strain interfaces for certain combinations of lattice parameters. More importantly, the results show that optimal phase boundaries may occur over a wide range of orientations depending upon small differences in the two lattices, which are sensitive functions of composition and perhaps pressure and temperature.

The results from this study provide important new information regarding the actinolite-hornblende system, and it can no longer be argued that there is no miscibility gap between these calcic amphiboles. The door is now open for more accurate delineation of the actinolite-hornblende gap, which will require detailed TEM and AEM studies of a variety of coexisting calcic amphibole assemblages as well as additional experimental studies.

ACKNOWLEDGMENTS

REFERENCES CITED

Aden, G.D., and Buseck, P.R. (1979) Rapid quantitative analysis of individual particles by energy dispersive spectrometry. In Dale Newberry, Ed., Microbeam analysis, p. 254–258. San Francisco Press, San Francisco.

Allen, J.M., and Goldie, R. (1978) Coexisting amphiboles from the Noranda area, Quebec: Extension of the actinolite-hornblende miscibility gap to iron-rich bulk compositions. American Mineralogist, 63, 205–209.

Bancroft, G.M., and Burns, R.G. (1969) Mössbauer and absorption spectral study of alkali amphiboles. Mineralogical Society of America Special Paper 2, 137–148.

Biermann, C., and Van Roermund, H.L.M. (1983) Defect structures in naturally deformed clinoamphiboles—A TEM study. Tectonophysics, 95, 267–278.

Binns, R.A. (1965) The mineralogy of metamorphosed basic rocks from the Willyama complex, Broken Hill district, New South Wales, Part I. Hornblendes. Mineralogical Magazine, 35, 306–326.

Bocchio, R., Ungaretti, L., and Rossi, G. (1978) Crystal chemical study of eclogitic amphiboles from Alpe Arami, Lepontine Alps, southern Switzerland. Societa di Italiana Mineralogia e Petrologia Rendiconti, 34, 453–470.

Bollman, W., and Nissen, H.-U. (1968) A study of optimal phase boundaries: The case of exsolved feldspars. Acta Crystallographica, A24, 546–557.

Brady, J.B. (1974) Coexisting actinolite and hornblende from west-central New Hampshire. American Mineralogist, 59, 529–535.

Cahn, J.W. (1961) On spinodal decomposition. Acta Metallurgica, 9, 795–801.

——— (1962) On spinodal decomposition in cubic crystals. Acta Metallurgica, 10, 179–184.

——— (1968) Spinodal decomposition. Transactions of the Metallurgical Society of AIME, 242, 166–180.

Cameron, K.L. (1975) An experimental study of actinolite-cummingtonite phase relations with notes on the synthesis of Fe-rich anthophyllite. American Mineralogist, 60, 375–390.

Champness, P.E., and Lorimer, G.W. (1971) An electron microscopic study of a lunar pyroxene. Contributions to Mineralogy and Petrology, 14, 171–183.

——— (1976) Exsolution in silicates. In H.-R. Wenk, P.E. Champness, J.M. Christie, J.M. Cowley, A.H. Heuer, G. Thomas, and N.J. Tighe, Eds., Electron microscopy in mineralogy, p. 174–204. Springer-Verlag, New York.

Charles, R.W. (1980) Amphiboles on the join pargasite-ferropargasite. American Mineralogist, 65, 996–1001.

Cho, M., Liou, J.G., and Bird, D.K. (1988) Prograde phase relations in the State 2-14 Well metasandstones, Salton Sea Geothermal Field, California. Journal of Geophysical Research, 93, 13081–13103.

Choudhuri, A. (1974) Distribution of Fe and Mg in actinolite, hornblende and biotite in some Precambrian metagraywackes from Guyana, South America. Contributions to Mineralogy and Petrology, 44, 45–55.

Christie, J.M., Lally, J.S., Heuer, A.H., Fisher, R.M., Griggs, D.T., and Radcliffe, S.V. (1971) Comparative electron petrography of Apollo 11, Apollo 12 and terrestrial rocks. Proceedings of the Second Lunar Science Conference, Geochimica et Cosmochimica Acta, 1 (suppl. 2), 69–89.

Christie, O.H.J., and Olsen, A. (1974) Spinodal precipitation in minerals and some new observations. Bullétin de la Société Français de Minéralogie et Cristallographie, 97, 202–205.

Colville, P.A., Ernst, W.G., and Gilbert, M.C. (1966) Relationships between cell parameters and chemical compositions of monoclinic amphiboles. American Mineralogist, 51, 1727–1754.

Cooper, A.F. (1972) Progressive metamorphism of metabasic rocks from the Haast schist group of southern New Zealand. Journal of Petrology, 13, 457–492.

Cooper, A.F., and Lovering, J.F. (1970) Greenschist amphiboles from Haast River, New Zealand. Contributions to Mineralogy and Petrology, 27, 11–24.

Dodge, F.C.W., Papike, J.J., and Mays, R.E. (1968) Hornblendes from granitic rocks of the central Sierra Nevada Batholith, California. Journal of Petrology, 9, 378–410.

Duebendorfer, E.M. (1988) Evidence for an inverted metamorphic gradient associated with a Precambrian suture, southern Wyoming. Journal of Metamorphic Geology, 6, 41–63.

Duebendorfer, E.M., and Houston, R.S. (1987) Proterozoic accretionary

tectonics at the southern margin of the Archean Wyoming craton. Geological Society of America Bulletin, 98, 554–568.

Ernst, W.G. (1966) Synthesis and stability relations of ferro-tremolite. American Journal of Science, 264, 37–65.

——— (1968) Amphiboles: Crystal chemistry, phase relations and occurrence, 125 p. Springer-Verlag, New York.

——— (1972) Ca-amphibole paragenesis in the Shirataki District, central Shikoku, Japan. Geological Society of America Memoir, 135, 73–94.

Fleet, M.E. (1981) The intermediate plagioclase structure: An explanation from interface theory. Physics and Chemistry of Minerals, 7, 64–70.

——— (1982) Orientation of phase and domain boundaries in crystalline solids. American Mineralogist, 67, 926–936.

——— (1984) Orientation of feldspar intergrowths: Application of lattice misfit theory to cryptoperthites and e-plagioclase. Bulletin de Minéralogie, 107, 509–519.

——— (1986) Lattice-misfit theory and transformation twinning in alkali feldspar. Canadian Mineralogist, 24, 615–623.

Fleet, M.E., and Arima, M. (1985) Oriented hematite inclusions in sillimanite. American Mineralogist, 70, 1232–1237.

Fleet, M.E., Bilcox, G.A., and Barnett, R.L. (1980) Oriented magnetite inclusions in pyroxenes from the Grenville Province. Canadian Mineralogist, 18, 89–99.

Gilbert, M.C. (1966) Synthesis and stability relationships of ferropargasite. American Journal of Science, 264, 698–742.

Gittos, M.F., Lorimer, G.W., and Champness, P.E. (1976) The phase distributions in some exsolved amphiboles. In H.-R. Wenk, P.E. Champness, J.M. Christie, J.M. Cowley, A.H. Heuer, G. Thomas, and N.J. Tighe, Eds., Electron microscopy in mineralogy, p. 238–247. Springer-Verlag, Berlin.

Graham, C.M. (1974) Metabasite amphiboles of the Scottish Dalradian. Contributions to Mineralogy and Petrology, 47, 165–185.

Graham, C.M., and Navrotsky, A. (1986) Thermochemistry of the tremolite-edenite amphiboles using flourine analogues, and applications to amphibole-plagioclase-quartz equilibria. Contributions to Mineralogy and Petrology, 93, 18–32.

Graham, C.M., Maresch, W.V., Welch, M.D., and Pawley, A.R. (1989) Experimental studies on amphiboles: A review with thermodynamic perspectives. European Journal of Mineralogy, 1, 535–555.

Grapes, R.H. (1975) Actinolite-hornblende pairs in metamorphosed gabbros, Hidaka Mountains, Hokkaido. Contributions to Mineralogy and Petrology, 49, 125–140.

Grapes, R.H., and Graham, C.M. (1978) The actinolite-hornblende series in metabasites and the so-called miscibility gap: A review. Lithos, 11, 85–97.

Hawthorne, F.C. (1981) Crystal chemistry of the amphiboles. In Mineralogical Society of America Reviews in Mineralogy, 9A, 1–102.

——— (1983) The crystal chemistry of the amphiboles. Canadian Mineralogist, 21, 173–480.

Hawthorne, F.C., and Grundy, H.D. (1973) The crystal chemistry of the amphiboles. I: Refinement of the crystal structure of ferrotschermakite. Mineralogical Magazine, 39, 36–48.

Hawthorne, F.C., Griep, J.L., and Curtis, L. (1980) A three-amphibole assemblage from the Tallan Lake Sill, Peterborough County, Ontario. Canadian Mineralogist, 18, 275–284.

Hietanen, A. (1974) Amphibole pairs, epidote minerals, chlorite, and plagioclase in metamorphic rocks, northern Sierra Nevada, California. American Mineralogist, 59, 22–40.

Jaffe, H.W., Robinson, P., and Klein, C. (1968) Exsolution lamellae and optic orientation of clinoamphiboles. Science, 160, 776–778.

Jaffe, H.W., Robinson, P., Tracy, R.J., and Ross, M. (1975) Orientation of pigeonite exsolution lamellae in metamorphic augite: Correlation with composition and calculated optimal phase boundaries. American Mineralogist, 60, 9–28.

Jenkins, D.M. (1988) Experimental study of the join tremolite-tschermakite: A reinvestigation. Contributions to Mineralogy and Petrology, 99, 392–400.

Kimball, K.L. (1988) High-temperature hydrothermal alteration of ultramafic cumulates from the base of the sheeted dikes in the Josephine Ophiolite, NW California. Journal of Geophysical Research, 93, 4675–4687.

Klein, C., Jr. (1969) Two-amphibole assemblages in the system actinolite-hornblende-glaucophane. American Mineralogist, 54, 212–237.

Leake, B.E. (1978) Nomenclature of amphiboles. American Mineralogist, 63, 1023–1053.

Litvin, A.L., Egorova, L.N., Michnik, T.L., Ostapenko, S.S., and Tepikin, V.E. (1972a) The structural refinements of actinolite and high-ferrous hornblende. Mineralogicheskii Sbornik, 26, 341–350.

Litvin, A.L., Egorova, L.N., Ostapenko, S.S., and Tepikin, V.E. (1972b) Comparative characteristics of hornblende structure from amphibolite and granulite metamorphic facies (Ukranian Shield). Konstitutsiya Svoistva Mineralov, 6, 3–14.

Litvin, A.L., Egorova, L.N., and Michnik, T.L. (1973) Cation distribution in two aluminous hornblendes from X-ray data. Konstitutsiya Svoistva Mineralov, 7, 31–35.

Livi, K.J.T., and Veblen, D.R. (1987) "Eastonite" from Easton, Pennsylvania: A mixture of phlogopite and a new form of serpentine. American Mineralogist, 72, 113–125.

McConnell, J.D.C. (1969) Electron optical study of incipient exsolution and inversion phenomena in the system $NaAlSi_3O_8$-$KAlSi_3O_8$. Philosophical Magazine, 19, 221–229.

——— (1974) Electron-optical study of the fine structure of a schiller labradorite. In W.S. McKenzie and J. Zussman, Eds., The feldspars. Proceedings of the NATO Advanced Study Institute, p. 378–424. Manchester University Press, Manchester, England.

Misch, P., and Rice, J.M. (1975) Miscibility of tremolite and hornblende in progressive Skagit metamorphic Suite, North Cascades, Washington. Journal of Petrology, 16, 1–21.

Mitchell, J.T., Bloss, F.D., and Gibbs, G.V. (1971) Examination of the actinolite structure and four other $C2/m$ amphiboles in terms of double bonding. Zeitschrift für Kristallographie, 133, 273–300.

Miyashiro, A. (1958) Regional metamorphism of the Gosaisyo-Takanuki district in the central Abukuma Plateau. Journal of the Faculty of Science, University of Tokyo, Section II, 11, 219–272.

Moody, J.B., Meyer, D., and Jenkins, J.R. (1983) Experimental characterization of the greenschist/amphibolite boundary in mafic systems. American Journal of Science, 283, 48–92.

Nord, G.L., Jr., Heuer, A.H., and Lally, J.S. (1974) Transmission electron microscopy of substructures of Stillwater bytownites. In W.S. McKenzie and J. Zussman, Eds., The feldspars. Proceedings of the NATO Advanced Study Institute, p. 522–535. Manchester University Press, Manchester, England.

——— (1976) Pigeonite exsolution from augite. In H.-R. Wenk, P.E. Champness, J.M. Christie, J.M. Cowley, A.H. Heuer, G. Thomas, and N.J. Tighe, Eds., Electron microscopy in mineralogy, p. 220–227. Springer-Verlag, New York.

Nyman, M.W., Tracy, R.J., and Law, R.L. (1989) Chemical and microstructural variation within an amphibolite shear zone as a function of shear strain. Eos, 70, 1391.

Oba, T. (1980) Phase relations in the tremolite-pargasite join. Contributions to Mineralogy and Petrology, 71, 247–256.

Oba, T., and Yagi, K. (1987) Phase relations on the actinolite-pargasite join. Journal of Petrology, 28, 23–36.

Owen, D.C., and McConnell, J.D.C. (1974) Spinodal unmixing in an alkali feldspar. In W.S. McKenzie and J. Zussman, Eds., The feldspars. Proceedings of the NATO Advanced Study Institute, p. 424–439. Manchester University Press, Manchester, England.

Papike, J.J., and Clark, J.R. (1968) The crystal structure and cation distribution of glaucophane. American Mineralogist, 53, 1156–1173.

Papike, J.J., Ross, M., and Clark, J.R. (1969) Crystal-chemical characterization of clinoamphiboles based on five new structure refinements. Mineralogical Society of America Special Paper 2, 117–136.

Raychaudhuri, B. (1964) Relation of atomic constitution to lattice parameters in some hornblendes from the Black Hills, South Dakota. American Mineralogist, 49, 198–206.

Robin, P.-Y.F. (1974) Stress and strain in cryptoperthite lamellae and the coherent solvus of alkali feldspars. American Mineralogist, 59, 1299–1318.

——— (1977) Angular relationships between host and exsolution lamellae and the use of the Mohr circle. American Mineralogist, 62, 127–131.

Robinson, P. (1963) Gneiss domes of the Orange Area, West Central

Massachusetts and New Hampshire. Ph.D. dissertation, Harvard University, Cambridge, Massachusetts.

Robinson, P., Jaffe, H.W., Klein, C., and Ross, M. (1969) Equilibrium coexistence of three amphiboles. Contributions to Mineralogy and Petrology, 22, 248–258.

Robinson, P., Jaffe, H.W., Ross, M., and Klein, C. (1971) Orientations of exsolution lamellae in clinopyroxenes and clinoamphiboles: Consideration of optimal phase boundaries. American Mineralogist, 56, 909–939.

Robinson, P., Ross, M., Nord, G.L., Jr., Smyth, J.R., and Jaffe, H.W. (1977) Exsolution lamellae in augite and pigeonite: Fossil indicators of lattice parameters at high temperature and pressure. American Mineralogist, 62, 857–873.

Robinson, P., Spear, F.S., Schumacher, J.C., Laird, J., Klein, C., Evans, B.W., and Doolan, B.L. (1982) Phase relations of metamorphic amphiboles: Natural occurrence and theory. In Mineralogical Society of America Reviews in Mineralogy, 9B, 1–227.

Ross, M., Papike, J.J., and Weiblen, P.W. (1968) Exsolution in clinoamphiboles. Science, 159, 1099–1102.

Ross, M., Papike, J.J., and Shaw, K.W. (1969) Exsolution textures in amphiboles as indicators of subsolidus thermal histories. Mineralogical Society of America Special Paper 2, 275–299.

Sampson, G.A., and Fawcett, J.J. (1977) Coexisting amphiboles from the Hastings region of southeastern Ontario. Canadian Mineralogist, 15, 283–296.

Shannon, R.D., and Prewitt, C.T. (1969) Effective ionic radii in oxides and flourides. Acta Crystallographica, B25, 925–946.

Shido, F., and Miyashiro, A. (1959) Hornblendes of basic metamorphic rocks. Journal of the Faculty of Science, University of Tokyo, Section II, 12, 85–102.

Smelik, E.A., and Veblen, D.R. (1989) A five-amphibole assemblage from blueschists in northern Vermont. American Mineralogist, 74, 960–965.

—— (1991) Exsolution of cummingtonite from glaucophane: A new orientation for exsolution lamellae in clinoamphiboles. American Mineralogist, 76, 971–984.

Spear, F.S. (1980) The gedrite-anthophyllite solvus and the composition limits of orthoamphibole from the Post Pond Volcanics, Vermont. American Mineralogist, 65, 1103–1118.

Tagiri, M. (1977) Fe-Mg partition and miscibility gap between coexisting calcic amphiboles from the southern Abukuma Plateau, Japan. Contributions to Mineralogy and Petrology, 62, 271–281.

Thompson, J.B., Jr. (1978) Biopyriboles and polysomatic series. American Mineralogist, 63, 239–249.

—— (1982) Composition space: An algebraic and geometric approach. Mineralogical Society of America Reviews in Mineralogy, 10, 1–31.

Vernon, R.H. (1962) Coexisting cummingtonite and hornblende in amphibolite from Duchess, Queensland, Australia. American Mineralogist, 47, 360–370.

Wenk, H.-R. (1971) Variations of lattice constants in clinoamphiboles. Zeitschrift für Kristallographie, 133, 341–363.

Whittaker, E.J.W., and Zussman, J. (1961) The choice of axes in amphiboles. Acta Crystallographica, 14, 54–55.

Willaime, C., and Brown, W.L. (1974) A coherent elastic model for the determination of the orientation of exsolution boundaries: Application to the feldspars. Acta Crystallographica, A30, 316–331.

Zussman, J. (1955) The crystal structure of an actinolite. Acta Crystallographica, 8, 301–308.

—— (1959) A re-examination of the structure of tremolite. Acta Crystallographica, 12, 309–312.